Study of γ ray induced showers at High Zenith Angles

Aitor Ibarra Ibaibarriaga

Trabajo de investigación dirigido por:

Victoria Fonseca

y

José Carlos González

Dpto. Física Atómica, Molecular y Nuclear
Facultad de Ciencias Físicas
Universidad Complutense de Madrid

Contents

Introduction

In the last ten years, the field of Cherenkov astronomy has become an important contributor to high energy astrophysics with the detection of eight objects at energies above 300 GeV. These observations have advanced our understanding of active galactic nuclei, supernova remnants, the extragalactic light background and cosmic-ray acceleration and production. Several efforts are now underway to develop new Cherenkov telescopes which will cover a wider range of energies (10 GeV - 100 GeV), improve the flux sensitivity by at least an order of magnitude and provide more accurate measures of particles energy and direction.

Gamma ray is the generic term applied to the rather extensive band of photons seen at the shortest wavelengths of the electromagnetic spectrum. This term was first applied to the penetrating radiation from radioactive atoms: this radiation has energies in the range of 1 to 5 megaelectron volts. Although the electromagnetic spectrum extends far beyond this, the same term *gamma ray* is used to describe even photons a million million times more energetic.

The Universe presents many constraining views when observed through different bands of the electromagnetic spectrum. Through the last decades astronomers had studied the universe from radio to gamma photons. In the optical range the sky is essentially populated by stable objects where stars and galaxies are the mayor components. At shorter wavelengths, X-ray and ultraviolet, a much more dynamic and unstable universe appears in which change is the rule rather than the exception. Finally, the gamma universe is violent, chaotic and explosive. Long before experiments could detect gamma-rays emitted by cosmic sources, scientists had known that the universe should be producing these photons. The study of the gamma spectrum show us a unique view of the hottest, most energetic regions of the cosmos. This view is also unique in that gamma-ray astronomy is an infant science and is currently in a period of discovery and vigor unparalleled in its history. In particular, the Energetic Gamma-Ray Experiment Telescope (EGRET) onboard the Compton Gamma Ray Observatory (CGRO) has moved the field from a few detections of a small number of sources to multi-faceted studies of several classes of Galactic and extra galactic objects.

Because gamma rays coming from space are mostly absorbed by the Earth's atmosphere they cannot be detected directly on ground, this being the reason for gamma-ray astronomy not to develop until it was possible to get our detectors above all or most of the atmosphere, using balloons or spacecrafts. The latest and relatively new technique for the study of gamma ray sources is the ground-based imaging air Cherenkov technique.

The imaging air Cherenkov technique is based on the detection of secondary particles originated when a cosmic-ray arrives to the Earth's atmosphere. When a cosmic-ray plungs into the atmosphere it produces a cascade of secondary particles which develop to the ground where they can be detected. This cascade receives the name of Extensive Air Shower or EAS. Among the particles produced in an EAS there is a charged component which is known to be responsible for the emission of a bluish light known as Cherenkov radiation. This radiation reaches the ground where the Cherenkov telescopes can collect it. Thus while energetic cosmic-rays themselves cannot reach the ground, the secondary particles and the Cherenkov photons they spawn can. For the search of gamma-ray sources the gamma photons have to be selected over the whole range of cosmic-rays that reaches the Earth's atmosphere, the so called hadronic background. This method is called γ/hadron separation and the improvement of the method is one of the main tasks of the Cherenkov Technique.

The Cherenkov radiation is a big source of information for the study of EAS and from this study we can obtain information such as the energy of the primary particle and point of origin of the gamma-ray on the celestial sphere.

A new important subject in EAS detection is the possibility to observe it at *High Zenith Angles* (HZA). This observations at HZA allow to extend the observation time window for any object seen at *Low Zenith Angles* (LZA), as well as to enlarge the dynamic energy range of an instrument towards the highest observable energies of γ-rays. The HZA technique requires: **detailed atmospheric extinction**, **proper EAS development at different energies and different zentih angles**.

For the study of EAS at HZA is very important a good knowledge of the atmospheric extinction. This will be studied in the *chapter 2*. For this work, we have made an atmospheric model, based on the *U.S. Standard Atmosphere, 1962* [24]. With this atmospheric model we calculate the transmission coefficients at different heights and for different wavelength. We have applied these transmission coefficients to EAS at different energies and at different zenith angles.

In the first part of the work, we have simulated γ-ray showers with two different energies: *Low energy EAS* (10 GeV and 100 GeV), and *high energy EAS* (3 TeV and 10 TeV, and for several zenith angles (0°, 40°, 60° and 80°). To do this, we had to modify our simulation programme (CORSIKA).

The goal of this work are the lateral distributions of Cherenkov photons for several zenith angles, and the absorptions curves obteined for several energies and several zenith angles (see chapter 3 and chapter 4).

Chapter 1

Physical Basis

1.1 Cherenkov Radiation

Cherenkov radiation was first observed in the early 1900's by the experiments developed by Mary and Pierre Curie when studying radioactivity emission. The nature of such a radiation, afterwards called Cherenkov radiation was unknown. The first attempt to understand the phenomenon was made by Mallet in 1926. He found that the light emitted from a wide variety of transparent bodies placed close to a radioactive source always had the same bluish-white quality, and the spectrum was continuous, not possessing the line or band structure characteristic of fluorescence. Mallet found such an emission but he could not find the nature of it.

It was not until the experimental work carried out between years 1934-1937 by P. A. Cherenkov and the theoretical interpretation by I. E. Tamm and I. M. Frank (1937) that this radiation was described, although it was not until 1958 that the effect was well understood and recognized. In the meanwhile lots of experiments were carried out. For example in 1947 the first experimental device was proposed by Getting for detecting single particles by the Cherenkov effect, and it is important to mention the first detection of Cherenkov radiation in a gas by Ascoli in 1953, or the observation of light pulses from the nigh sky by Galbraith and Jelley in 1953, experiments that started the search for Cherenkov radiation in the atmosphere.

It is not the aim of this work to give a complete mathematical description of the Cherenkov effect. Rather than that a more qualitative description will be given for a better understanding of future references.

The Cherenkov radiation is produced when a charged particle moves in a transparent medium (understanding by transparent medium the one in which the absorption coefficient is zero and thus the refraction index is real) at a speed higher that the speed of light in the medium.

Before starting the description of the Cherenkov effect it must be emphasized that the Cherenkov radiation is entirely unrelated to the bremsstrahlung, which is emitted by the moving electron itself when it collides with atoms in the medium. The Cherenkov effect involves radiation emitted by the medium under the action of the field of the particle moving in it. The distinction between the two types of radiation appears with particular clarity when the particle has a very large mass: bremsstrahlung disappears, but the Cherenkov radiation is unaffected.

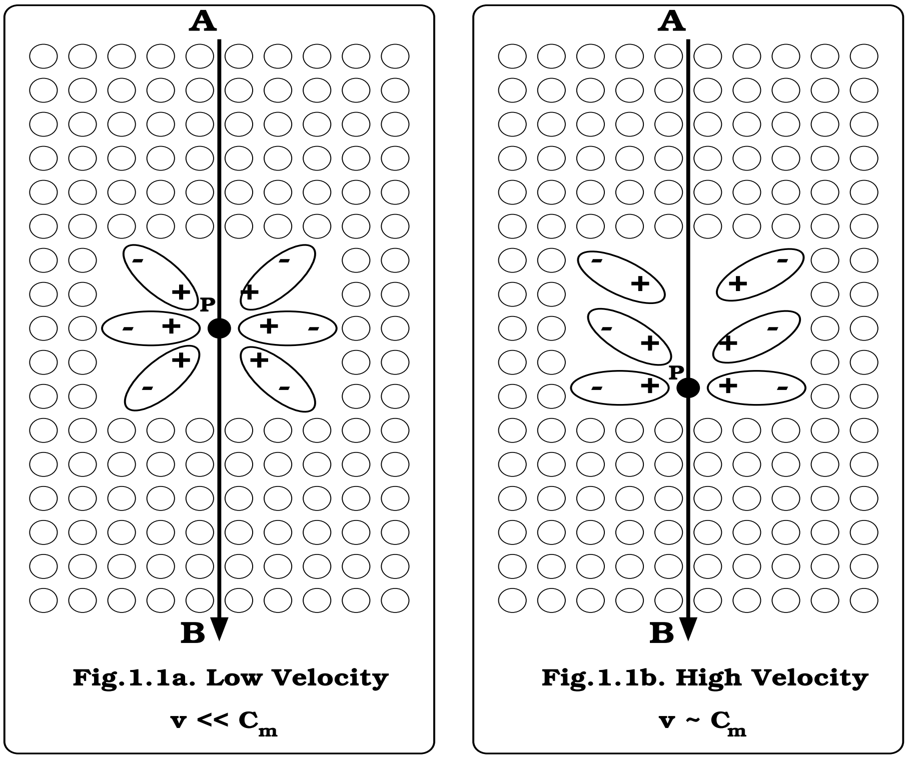

Figure 1.1: *The polarization set up in a dielectric when a charged particle passes through.*

Let's illustrate two cases, an electron moving slower than the speed of light and an electron moving at a speed faster than the speed of light through a piece of glass or other transparent medium. For the first case Fig.(1.1a) shows a section of the glass in the vicinity of the track AB of this electron, the circles represent the individual atoms composing the glass. At a certain time the particle is in point P, the electric field of the particle distorts the atoms so that the positive charges are displaced towards the moving electron and the negative charges of the nuclei are displaced to the other side. The medium thus becomes polarized about the point P. When the electron moves to point P' the atoms in point P return to the normal position radiating electro-magnetic pulses. We can say that the electron polarizes the medium as it goes through it leaving regions of instant dipoles. Owing to the complete symmetry of the polarization field surrounding the electron, there will be no resultant field and thus no emission at large distances. If we take a look at Fig.(1.1a) we can see that there is symmetry both in azimuth and along the axis AB.

If, however, the electron is moving fast the situation is quite different as you can see in Fig.(1.1b). In the azimuthal plane, symmetry is preserved, but along the axis there is a resultant dipole field which will be apparent even at large distances from the track of the electron. Such a field will be momentarily set up by the electron at each element along the track, in turn each element will radiate a brief electro-magnetic pulse. The waves coming form each element of the track interfere constructively being the reason for the existence of a resultant field not equal to zero.

The reason why there is a dependence in the emission of Cherenkov radiation with the velocity of the particle is the following. The instant dipoles in the medium are set by the electro-magnetic field of the particle moving. When the particle moves slower than the speed of light the electro-magnetic waves travel ahead of the particle setting instant dipoles in the medium before the particle reaches those regions (see Fig.(1.1a)). That is the reason why no net polarization is set along the track of the particle. When the particle moves at a speed higher than the speed of light in the medium no instant dipoles are set ahead of the particle because the particle travels at a speed greater than the electro-magnetic waves emitted by the particle (see Fig.(1.1b)). This sets instant dipoles along the track of the particle being the reason for the existence of a net polarization along the track of the particle.

In Fig.(1.2) a geometrical interpretation of the emission of the Cherenkov radiation is shown.

From this figure it is understood that this radiation is only observed at a particular angle Θ called Cherenkov angle, with respect to the track of the particle. This angle represents the position in which waves from arbitrary point such as P1, P2 and P3 over the track AB are coherent and combine to form a plane wave front BC. This coherence takes place when the particle travels from A to B in the same time that the light travels from A to C. If the velocity of the particle is v or $\beta\cdot$ c where c is the velocity of light *in vacuo* and $\frac{c}{n}$ is the velocity of the

Cherenkov light in the medium, then we can write the Cherenkov angle in the following way only taking into account geometrical considerations:

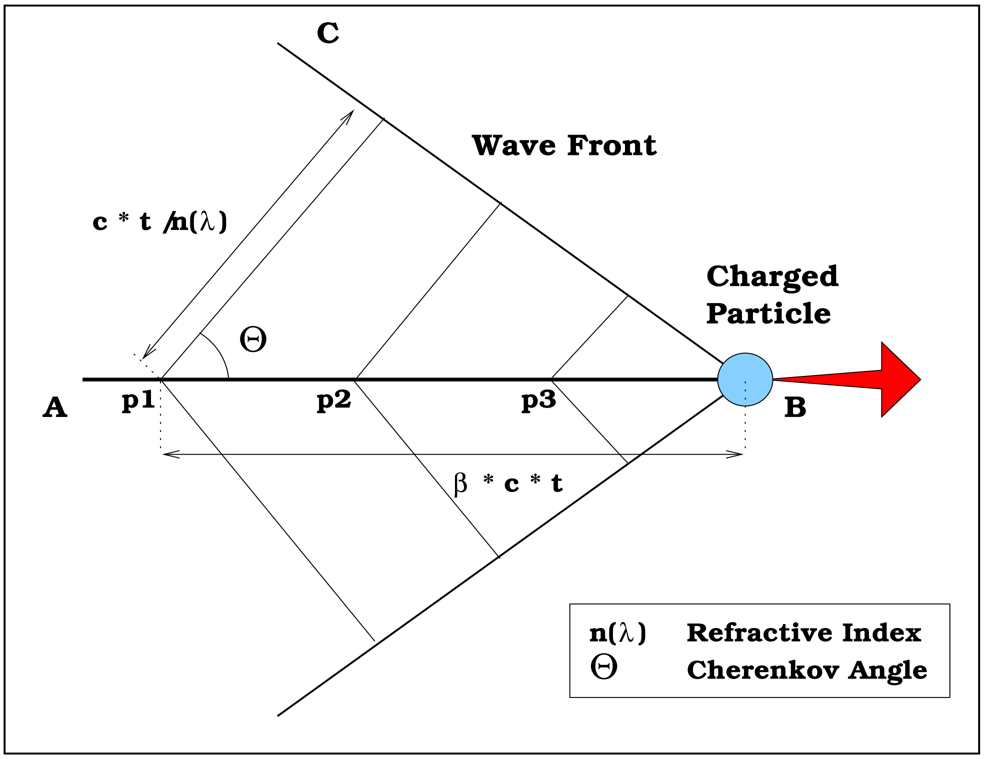

Figure 1.2: *Huygens construction to illustrate coherence.*

$$\cos\Theta = \frac{\frac{c}{n(\lambda)} \cdot \Delta T}{\beta \cdot c \cdot \Delta T} \tag{1.1}$$

$$\boxed{\cos\Theta = \frac{1}{\beta \cdot n(\lambda)}} \tag{1.2}$$

where n is the refractive index of the medium and ΔT is the time in which the particle moves from A to B.

From equation (1.2) we can take out some particular implications:

- (i) For a medium of a given refractive index n, there is a threshold velocity $\beta_{min} = \frac{1}{n}$, below which no radiation takes place. At this critical velocity the direction of radiation coincides with that of the particle. To see this we could write (1.2) in the following way:

$$\cos\Theta = \frac{1}{\beta \cdot n(\lambda)} = \frac{c_{medium}}{v_{part}} \tag{1.3}$$

so when v_{part} is lower than c_{medium} the equation does not have solution, and no radiation takes place.

We can see all this from a different point of view. The wave vector and frequency of an electro-magnetic wave propagating in a transparent medium are related by $k = \frac{nw}{c}$, where n is again the refractive index. The frequency of the field created by a particle moving uniformly in the x-direction in a medium is related to the x-component of the wave vector by $w = k_x \cdot v$. If this component is a freely propagated wave, these two relations must be consistent. Since k $> k_x$ it follows that we must have,

$$v > \frac{c}{n(\omega)} \tag{1.4}$$

Thus radiation of frequency ω occurs if the velocity of the particle exceeds the phase velocity of waves of that frequency in the medium concerned. On the other hand we have the relation between k and k_x:

$$k_x = k \cdot cos\Theta = \frac{nw}{c} \cdot cos\Theta \tag{1.5}$$

where, as we just show, cos $\Theta = \frac{c}{nv}$.

So when $\frac{c}{nv} \sim 1$ then $\Theta \sim 0$ and $k_x \sim$ k, that is, the direction of radiation coincides with that of the particle.

- (ii) For an ultra-relativistic particle, for which $\beta = 1$, there is a maximum angle of emission, given by,

$$\cos\Theta = \frac{1}{n} \tag{1.6}$$

- (iii) The radiation occurs in the visible and near visible regions of the spectrum, for which $n > 1$. A real medium is always dispersive, so actually radiation is restricted to those frequencies bands for which $n(\omega) > \frac{1}{\beta}$. In the x-ray region $n(\omega)$ is always < 1 and radiation is forbidden. So emission in the x-ray region is impossible for n is less than unity and equation (1.6) cannot be satisfied.

There are two further conditions to be fulfilled to achieve coherence, in addition to that stated in point (i). First, the length l of the track of the particle in the medium should be large compared with the wavelength λ of the radiation in question, otherwise diffraction effects will become dominant. Secondly, the velocity of the particle must be constant during its passage through the medium, or, to be more specific, the differences in the times for particle to traverse successive distances λ should be small compared with the period $\frac{\lambda}{c}$ of the emitted light. If we take into consideration the Maxwell theory of electro-magnetic waves a charged particle moving uniformly does not irradiate and this is the prove that the Cherenkov radiation is not related with Bremsstrahlung.

We would like to underline the following point as being important for further explanations. The Cherenkov radiation originated in each element of the track is propagated along a surface of a cone whose apex is at the element, whose axis coincides with the track, and whose semi-vertical angle is the angle Θ.

The number of photons emitted by a charged particle of charge **ze** per unit path length and per unit energy interval, or equivalently to λ, of the photons is equal to:

$$\boxed{\frac{dN^2}{dx d\lambda} = \frac{2\pi\alpha z^2}{\lambda^2} \cdot \left(1 - \frac{1}{\beta^2 \cdot n^2(\lambda)}\right)} \tag{1.7}$$

For the particular case of an electron moving along a track of length l within a spectral region defined by wavelengths λ_1 and λ_2 we will have:

$$\boxed{N = 2\pi\alpha l \cdot \left(\frac{1}{\lambda_2} - \frac{1}{\lambda_1}\right) \cdot \left(1 - \frac{1}{\beta^2 \cdot n^2(\lambda)}\right)} \tag{1.8}$$

where α is the structure constant $= \frac{e^2}{\hbar \cdot c} = \frac{1}{137}$ and n is the refraction index of the medium that is a function of the photon energy, or equivalently of λ.

The spectral distribution of the radiation may be expressed in several ways. Since the intensity of light of frequency ν, or $\frac{\omega}{2\pi}$, may be written as $\mathbf{W} = N \cdot h\,\nu$ where h is the Plank's constant, the spectral distribution may be written in any of the following four ways:

$$\frac{d^2W}{dldw} \propto w \tag{1.9}$$

energy per unit path and frequency interval

$$\frac{d^2W}{dld\lambda} \propto \frac{1}{\lambda^3} \tag{1.10}$$

energy per unit path and wavelength interval

$$\frac{d^2N}{dldw} \propto const \tag{1.11}$$

number of photons per unit path and frequency interval

$$\frac{d^2N}{dld\lambda} \propto \frac{1}{\lambda^2} \tag{1.12}$$

number of photons per unit path and wavelength interval

The energy carried off by Cherenkov radiation can be written in the following way,

$$-\frac{dE}{dx} = \frac{4\pi e^2}{c^2} \int w dw \left(1 - \frac{1}{\beta^2 \cdot n^2}\right) \tag{1.13}$$

where the integration is only over those frequencies for which $\beta \cdot n(w) > 1$.

1.2 Extensive Air Showers

It was not until 1927 that all doubt was removed about the existence of what initially was called cosmic-radiation and not until 1948 when the nature of such a radiation began to be understood. By *Cosmic Radiation* (CR) we understand all kinds of particles and high energetic radiation reaching the Earth from the outer space. Basically the cosmic radiation is integrated by atomic nuclei (96% H, 3% He, 1% C,N,O,Fe), γ-rays, electrons and positrons, neutrinos and other types of elemental particles. Nowadays only charged particles and nuclei with sufficiently high energies are called cosmic-rays. In the following figure (Fig.1.3) the spectrum of comic-rays is plotted. The cosmic-ray spectrum extends in energy up to at least 10^{20} eV.

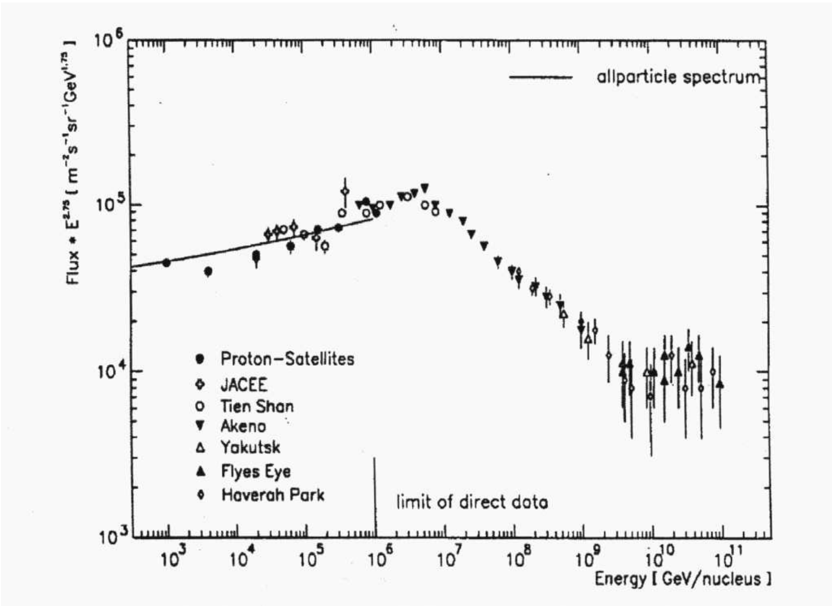

Figure 1.3: *The energy spectrum of cosmic radiation.*

The cosmic radiation travels from the emission source until it reaches the Earth. On its way through the outer space some interactions with the intergalactic or interstellar medium can take place, as for example fragmentation of the nuclei, ionization, particle production and many more. This sub-products of the original cosmic particles are the ones that reach the Earth's atmosphere. When the cosmic rays enter the earth's atmosphere they have extremely high energy and give rise to a number of complicated processes through the interaction with an atmospheric nucleus that gives rise to a certain number of *secondary particles* turning into what is called Extensive Air Shower or EAS. The secondary particles experiment more interactions through the atmosphere. there are two kinds of these intereactions depending on the nature of the particles; interaction *charged particle-matter* and interaction *radiation-matter*. For the first case two principle features characterize the passage of charged particles through matter: (1) a loss of energy by the particle and (2) a deflection of the particle from its incident direction. These effects are primarily the result of two processes:

- *inelastic collisions* with the atomic electrons of the material where energy is transferred from the particle to the atom causing an ionization or excitation of the latter.
- *elastic scattering* from nuclei, where the charged particle experiments successive elastic collision in the field of a nuclei. In general very little energy is transfered in these collisions.

These, however, are not the only reactions which can occur. Other processes include,

- emission of *Cherenkov radiation.*
- *nuclear reactions.*
- *bremsstrahlung.*

For the second case, interaction radiation-matter, three effects can take place:

- *photoelectric effect.* Dominant at energies E $\leq$ 100 KeV.
- *Compton scattering.* Dominant at energies around 1 TeV.
- *pair production.* Begins to be important at energies higher than 1 MeV and it is the dominant effect at energies higher than 25 MeV.

The final result of all these processes that take place with the arrival of a cosmic-ray is a shower of particles that travels through the atmosphere until they reach the ground. It has to be mentioned that the shower does not keep growing until it reaches the ground. In every process the energy per particle is reduced so the shower gets to a critical point where dissipation processes become more important than creation processes and the shower begins to extinguish.

As already mentioned, among these high energy particles reaching the Earth there is a small flux of gamma-rays: about 1 out 1000 air showers produced in the atmosphere are gamma initiated. There are some differences in the development of an air shower depending on the primary particle originating the shower. Let's take a look at both cases, a gamma-ray initiated shower and an hadronic initiated shower.

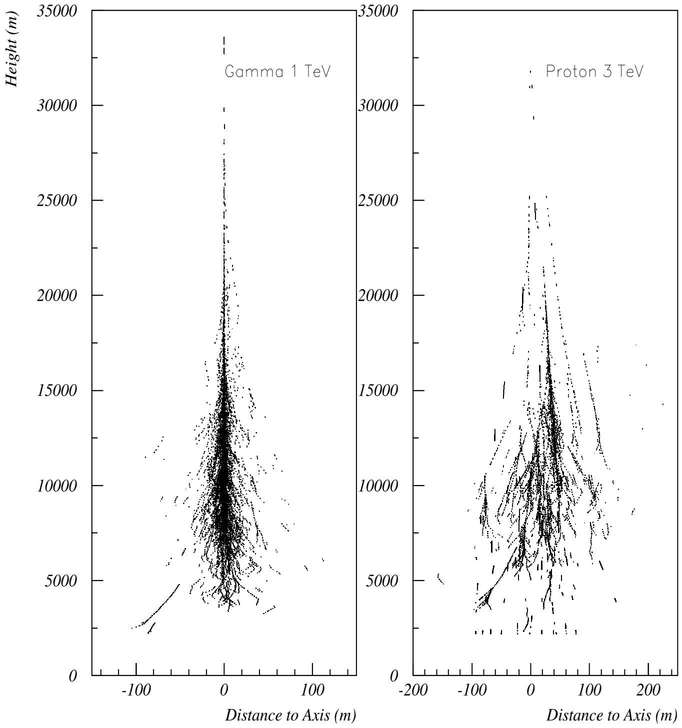

Figure 1.4: *Gamma initiated shower of energy 1 TeV and proton shower of energy 3 TeV.*

- *Gamma-ray Initiated Shower*: At the energies involved in the process that take place in the upper atmosphere when a γ-ray plunges into the atmosphere the pair production is the dominant effect. This is the situation in EAS. The process of pair production takes place in the field of an atmospheric nuclei or electron in order to conserve momentum. A high energy photon, of at least an energy of 1.022 MeV, in matter converts into an electron and positron pair with half of the energy each. If the energy is sufficient, the resulting electron-positron pair does not quickly lose its energy by ionizating interactions. Instead, an electron in the field of a nucleus can produce a secondary gamma ray. This process is called bremsstrahlung. This gamma ray, if its energy is still higher than 1.022 MeV, can then produce another electron-positron pair that can undergo further bremsstrahlung interactions. The result is a cascade of photons, electrons and positrons, which continues traveling in the original direction of the primary gamma ray and sharing its total energy.

We are going to take a closer look at the gamma-ray initiated shower. A simple model ([18, M.S. Longair 1992]) could be made to explain the processes that take place when a gamma-ray reaches the atmosphere.

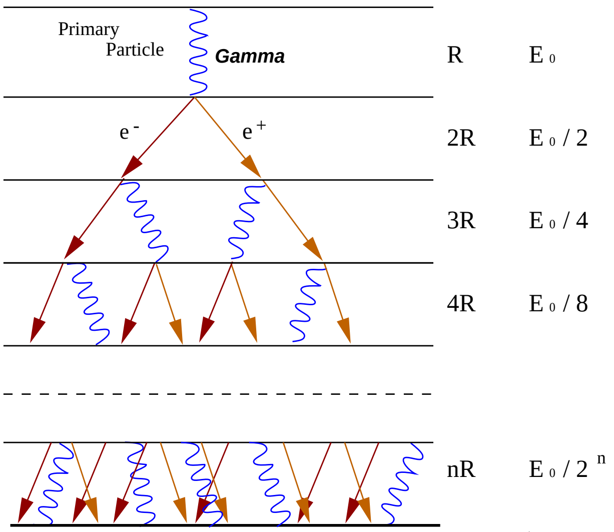

Figure 1.5: *Model of an electro-magnetic shower.*

Let us assume that an incident photon of energy E_0 traverses a distance R before creating an electron-positron pair. This distance can be expressed in terms of radiation length. One *radiation length* is the mean distance over which a high energy electron loses all but $1/e$ of its energy by

Bremsstrahlung. At these high energies this is also the distance a beam of gamma photons must traverse so that all but $1/e$ of them have produced an $e^{\pm}$ pair. For the atmosphere this quantity equals $\xi_0 \simeq 36.7$ g/cm^2. So actually R = $\xi_0 \cdot \ln 2$, in terms of radiation lengths. The probability of a photon or electron to interact along a distance R is therefore, exp(-R/ξ_0) = 1/2. It is considered that in each interaction the energy is equally divided between $e^{\pm}$ and γ's. Then in the first interaction each particle has half of the initial energy on the average. After traveling another distance R, each particle will bremsstrahlung and produce a photon of average energy $\frac{E_0}{4}$. At a distance nR into the shower, there will then be 2^n particles created, each with an average energy $\frac{E_0}{2^n}$. This multiplicative process continues until the average energy of the particle drops bellow some energy E_c, called the *critical energy*. This energy is defined as the energy below which the dominant energy loss is by ionization, via atomic collisions, rather than by bremsstrahlung emission, thus halting the cascade. This energy in the air is around 81 MeV per particle. At this point, no further multiplication occurs except for very low energy electron-ion pair production. For γ rays, the critical energy correspond to a point where Compton scattering begins to be more important than pair production.

Critical energy:

$$\text{photons} \rightarrow \sigma_{com} \approx \sigma_{pair}$$

$$e^{\pm} \rightarrow (\tfrac{dE}{dx})_{rad} \approx (\tfrac{dE}{dx})_{col}$$

The shower thus reaches its maximum development when the average energy of the cascade particles equals the critical energy. The total number of photons and electrons at the shower maximum is then given by the total energy E_0 divided by the critical energy E_c.

$$N_{max} = \frac{E_0}{E_c} \tag{1.14}$$

The maximum penetration depth of the cascade X_{max}, if we assume that the shower stops abruptly at the critical energy E_c, is,

$$E(X_{max}) = \frac{E_0}{2^n} = E_c \tag{1.15}$$

which solving for n, gives a value for X_{max}, as a function of primary energy and ξ_0,

$$X_{max} = \frac{Ln\frac{E_0}{E_c}}{Ln2} \cdot R = Ln\frac{E_0}{E_c} \cdot \xi_0 \tag{1.16}$$

A better approximation for the number of particles ($e^{\pm}$) produced in a shower as a function of the primary energy and atmospheric depth, is given by Greisen equation (1.17) ([19, K. Greisen 1956]). In figure Fig.(1.6) is represented the number of shower particles ($e^{\pm}$) in terms of the atmospheric depth (measured in radiation lengths) with the aid of:

$$N_e(t) = \frac{0.31}{\sqrt{ln(E_0/E_c)}} \cdot \exp t \cdot (1 - 1.5 \quad lns) \tag{1.17}$$

where $s = \frac{3 \cdot t}{t+2ln(E_0/E_c)}$ is known as the age parameter that indicates the degree of development of the shower, and t is the atmospheric depth in terms of radiation length. A value of s = 0 indicates the first interaction point, s = 1 indicates the maximum development of the shower and s = 2 the point in which the shower begins to extinguish.

This models, of course, only give a rough qualitative picture of the shower. In reality, the number of particles in an electro-magnetic shower rises exponentially to a broad maximum after which it declines gradually. In general, a precise calculation cannot be made analytically and recourse must be made to such techniques as Monte Carlo simulations.

- *Hadronic Initiated Shower*: These particles, most of which are protons, cause nuclear disintegration at the top of the atmosphere, with the emission of further particles which in turn themselves produce disintegrations. We could write this interaction in the following way:

  Cosmic Ray (CR) + Atmospheric Nuclei (AN) $\Rightarrow$ CR' + AN' + n$\pi^{\pm}$ + mπ^0 + other mesons.

  where CR' is a fragment of the original cosmic ray that can keep producing more interaction with atmospheric nuclei. If the original cosmic ray has enough energy some of its fragments could reach the ground. AN' are fragments of atmospheric nuclei in a high energy state. Among the products of the nuclear disintegrations are the π-mesons, which can decay in the following sub-products,

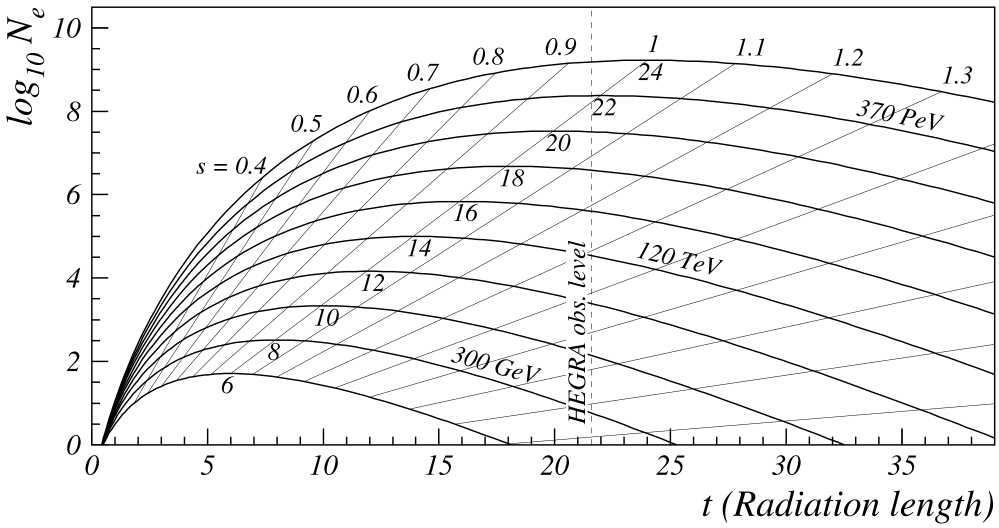

Figure 1.6: *Longitudinal development of an atmospheric shower in terms of atmospheric depth according to the Greisen approximation. Different curves represent different energies of primary photons E_0. The value $ln(E_0/E_c)$ are shown under the curves. At sea level the atmospheric depth is around 27 radiation lengths.*

$$\pi^0 \rightarrow 2\ \gamma \qquad \tau = 1.8 * 10^{-16} s$$
$$\pi^\pm \rightarrow \mu^\pm + \nu_\mu \qquad \tau = 2.5 * 10^{-8} s$$
$$\mu^\pm \rightarrow e^\pm + \nu_e + \nu_\mu \qquad \tau = 2.2 * 10^{-6} s$$

The decay of the π^0 in two high energy γ-rays originates what it is called the electro-magnetic component of the shower because from here on only electrons and γ-rays will be produced having a component made up by electrons and gammas by the processes of bremsstrahlung and pair production. The process by which this sub-cascade develops is the same as the one describe for the pure electro-magnetic showers. The whole process is summarize in the next figure.

Let's take a more qualitative look at the differences between an hadronic initiated shower and a gamma-ray initiated shower on the basis of the longitudinal and transversal development and the implications of this development on the pattern left on ground by the Cherenkov radiation. The knowledge of the longitudinal development of the shower it is important to understand the polarization vector distribution on ground and the existence of a net polarization.

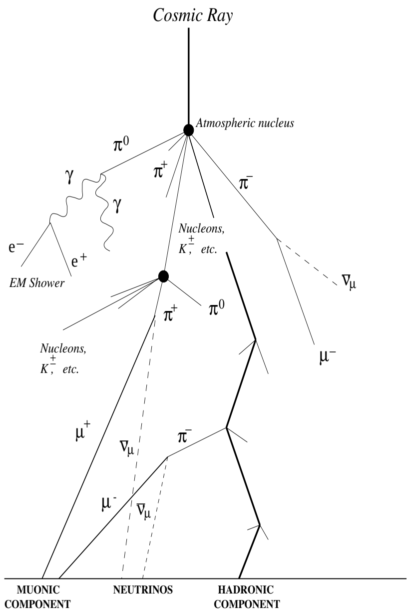

Model of an Extensive Air Shower initiated by a cosmic ray.

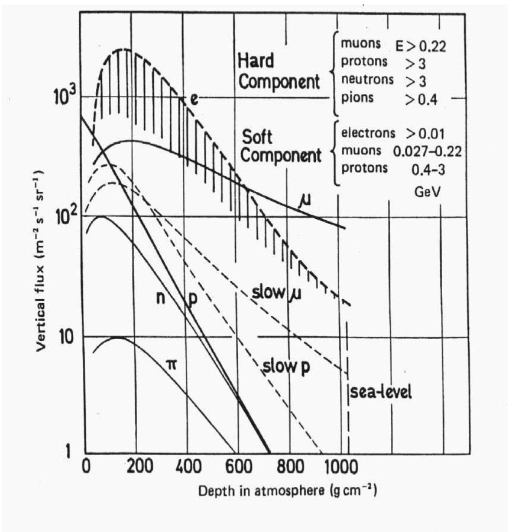

The vertical fluxes of different components of cosmic rays within the atmosphere.

1.3 Cherenkov Radiation in EAS

For primary energies less than 20 TeV the cascades die out in the upper atmosphere but the Cherenkov radiation produced by the charged component of the shower, penetrates to ground level where it might be collected. Although subject to fluctuations in the point of origin of the cascade and its subsequent development, the Cherenkov light carries with it information pertaining to the exact point of origin of the primary γ-ray on the celestial sphere and also the energy of the primary particle.

In electro-magnetic showers electrons and positrons are the main charged component that radiates Cherenkov light. This is true if the energy of this particles exceeds a minimum threshold E_{min}, as can be pointed out from equation (1.20). This threshold is 21 MeV at see level and increases to 35 MeV at 7.5 kilometers above sea level. The reason for this change in the E_{min} is the variation of the Cherenkov threshold velocity with index of refraction of the atmosphere. We can make an estimation of E_{min} an its dependence with the index of refraction. We know that the velocity of the light in a certain medium is given by,

$$v = \frac{c}{n(H)} \tag{1.18}$$

where c is the speed of light *in vacuum* and n is the refraction index at a given atmospheric height H.

We can then write E_{min} in the following way, where E_{min} is the energy of a relativistic particle moving along a medium at a certain speed,

$$E_{min} = m_0 \cdot c^2 + E_c = \gamma_{min} \cdot m_e \qquad \gamma_{min} = \frac{1}{\sqrt{1 - \frac{1}{n^2}}} \tag{1.19}$$

so if we write n = 1 + δ, with $\delta << 1$, then $\gamma_{min} \approx \frac{1}{\sqrt{2\delta}}$, so

$$\boxed{E_{min} \approx \frac{m_e}{\sqrt{2\delta}}} \tag{1.20}$$

We can approach the study the Cherenkov radiation in an EAS in terms of the longitudinal development of the EAS, or in terms of the lateral distribution of shower particles. The longitudinal spread of the shower is the distribution in points of emission of Cherenkov photons with height.

The lateral distribution of an EAS in terms of Cherenkov radiation is the study of the emission points of Cherenkov radiation in planes perpendiculars to the shower axis. The lateral distribution is thus sensitive to the longitudinal shower development. On the basis of the lateral distribution we can say that steep lateral distributions are associated with showers which develop close to the observer, while showers developing high in the atmosphere have broader distribution exhibiting a characteristic pattern on ground called *Cherenkov ring* that will be discuss now.

The angle of maximum emission of Cherenkov light with respect to the particle direction varies with height because of the change in the refraction index with height, and is given by,

$$cos(\Theta_{max}) = \frac{1}{n} = \frac{1}{1+\delta} \simeq 1 - \delta \tag{1.21}$$

We can then approximate Θ_{max} (rad) $= \sqrt{2\delta}$. With this value we can establish a relation to obtain the distance R_{core} between emitted Cherenkov photons and the particle trajectory at a certain observation height h_{obs}:

$$R_{core} \equiv (h - h_{obs}) \cdot tan(\Theta_{max}) \tag{1.22}$$

The values for R_{core} were obtained for an ultrarrelativistic electron of vertical incidence and for two observation levels, the one corresponding to the HEGRA experiment, h_{obs}=2200. m, and for the sea level. We can see that R_{core} has a maximum between 10 and 20 km. This makes all the Cherenkov light emitted by the particle between this two heights to reach the observation level in a ring at a distance R_{core}, of around 120 m. (sea level).

For a single relativistic particle radiating high in the atmosphere, the Cherenkov angle is less than a degree, but opens to about 1 degree at 8 km altitude and, due to greater air density, opens to about 1.5 degrees at see level.

The variation of the Cherenkov angle with height combined with the fact that the emitting particles move towards the ground gives rise to a geometrical effect. If all the charged particles move along the shower axis, with no lateral displacement, the light would be emitted at the characteristic Cherenkov angle, which is around 1 degree. As the emitting particle speeds up to ground the Cherenkov angle opens focusing the Cherenkov radiation into a narrow annular strip. As an approximation, for a 1 TeV gamma shower the light generated from heights between 6 to 10 kilometers above sea level would fall on ground within a ring of 110 to 145 meters in radius from the shower impact point on ground, if electrons did not multiple scatter. Electron multiple scattering broadens this Cherenkov ring but does not totally eliminate it. We can see the effect in the above figure, 50 % of the light is generated between 6 to 10 km and falls in what is called the hump of the Cherenkov pool. The other 50 % is split equally between both higher and lower altitudes. For a proton cascade of the same primary energy the same column is represented in dashed line. The Cherenkov ring is most prominent when the shower dies out far above the observation level, as in low energy gamma showers. The intensity near the shower axis rises when the tail of the shower penetrates close to the observation level, like at high energies, because light emitted closer to the ground has a shorter distance to travel, out weighting the somewhat larger Cherenkov angle, and so it strikes the ground closer to the axis.

As can be seen in the figure above of the lateral distribution, every radial distance on ground from the core, represents a different atmospheric height: the main bulk of particles particles, near shower maximum, produces the light seen at 100-130m from the shower axis; close to the shower axis (within 40m) one sees the light from local particles, the tail of the shower.

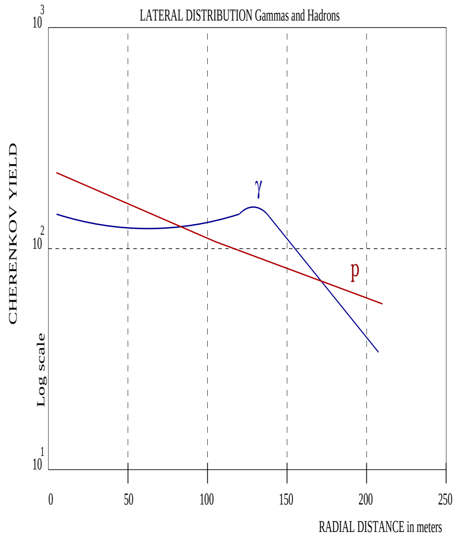

Lateral distribution of Cherenkov light yield on the ground for typical γ-ray and hadron showers. The γ-ray induced shower shows a relatively flat lateral distribution of light out to about 125m radial distance from the center.

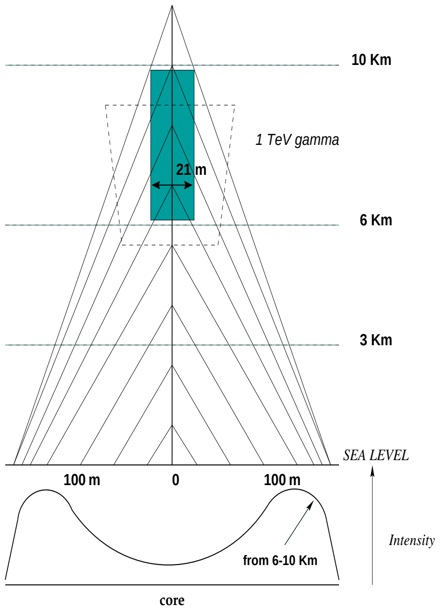

Geometric model of emission of Cherenkov radiation for γ-ray and hadron showers. The stippled region encloses the main emission region for production of Cherenkov light from γ-ray showers. The intensity profiles on the ground reflect the peaking in the Cherenkov lateral distribution for γ-ray showers at distances to about 126 m from the center of the light pool.

When the lateral distribution of light for different energies is compared, the hump (Cherenkov ring) has been shown to be due to high energy electrons above 1 GeV (see chapter 4). Electrons of lower energies are more scattered and the Cherenkov ring is washed out.

Another important fact of the Cherenkov radiation is the pulse shape. The Cherenkov pulse shape seen at a distance R from the core depends on the shower geometry and shower development, as well as on the variation of the refractive index with altitude. Simulation shows that at small core distances Cherenkov light produced low in the atmosphere reaches the ground first (see Fig.(1.7)). We can assume that light reaching ground at a given time t comes from a particular atmospheric height.

Lets now comment some differences between gamma initiated showers and

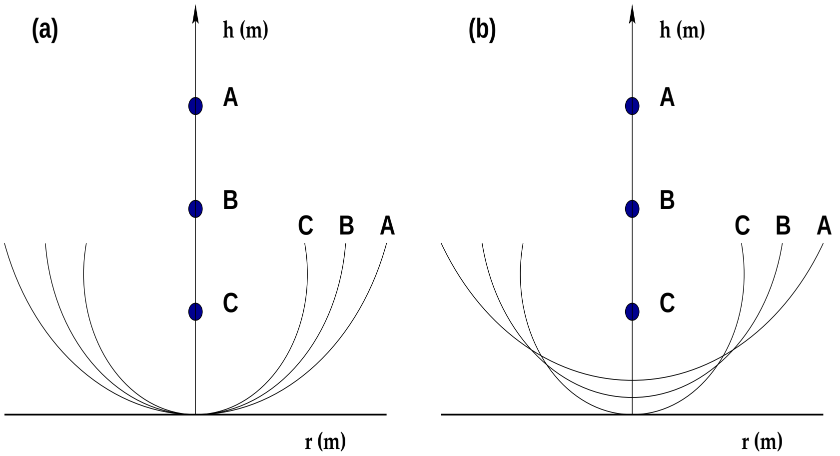

Figure 1.7: *Shapes of Cherenkov light fronts:(a) assuming no variation of atmospheric index of refraction; and (b) realistic case.*

hadron initiated shower. The interaction length for a primary proton in the atmosphere is about 80 gm cm^{-2} compared to about 38 gm cm^{-2} for γ rays, therefore proton showers will develop further into the atmosphere. By propagating much further into the atmosphere, the proton induced shower carries a Cherenkov component much closer to the ground level than γ induced showers, and this is reflected in a more intense pool of Cherenkov light close to the shower axis not presenting the ring shown in gamma initiated showers.

On the basis of the longitudinal development proton showers show much greater shower to shower fluctuations than gamma showers because a greater number of process can take place in the first ones, making the longitudinal development more chaotic and unpredictable. About the lateral distribution we could say that because of high transverse momentum flow to pions arising in the strong interactions, the hadronic shower will show a greater transverse development at all points of its longitudinal development than gamma showers as can be seen in (Fig.(1.4)). This will have further implication in the analysis of the images left on a detector by an extensive air showers as we will see further on.

One interesting feature of the Cherenkov pool left by gammas is the regularity of it in contrast to the hadron one that shows more irregularities. We can find the reason for this if we take a look at the longitudinal development of the hadronic initiated showers. As we saw earlier when a cosmic ray enters the atmosphere among other particles three types of pi-mesons can appeared. Only the neutral pion can decay to produce γ-ray pairs, thus sustaining electro-magnetic processes within the cascade. In first order approximation we could say that 1/3 of the energy of the primary particle goes to the electro-magnetic component of the shower. So in principle for the same primary energy hadronic showers will show a Cherenkov pool on ground less intense. On the other hand, in hadronic showers there is other sources of Cherenkov emission other than electrons and positrons that contribute to the Cherenkov pool as can be the muons. This muons do penetrate to the ground over a wide area and an intense local peak of Cherenkov light is seen around each muon impact point.

1.4 The Atmosphere

To describe the interaction of the earth's atmosphere with EAS, it is essential that the atmosphere's composition is understood. The atmosphere is composed of a group of nearly *permanent* gases and a group of gases with variable concentration. In addition, the atmosphere also contains various solid and liquid particles such as aerosols, water drops, and ice crystals, which are highly variable in space and time.

The atmosphere is too large and too complex to ever be fully described, so any description can only be an approximate model. The atmosphere is divided into different layers: Troposphere, Stratosphere, Mesosphere, Thermosphere and Exosphere. The more important layers for our study are the Troposphere and the Stratosphere. The layers where we have the development of the EAS are the Troposphere, Stratosphere and the lowest parts of the Mesosphere, so we should look at these layers carefully.

The Stratosphere is the layer where the biggest amount of ozone is located. Although the ozone is a minor constituent (N_2 and O_2 molecules are the major constituents) it has a big cross section, so its effect in the absorption is larger. Approximately 90% of the ozone in the atmosphere resides in the Stratosphere. In the model we have used to simulate the atmospheric attenuation (see chapter 2) [24] the biggest amount of ozone is located between 20 and 25 Km.

The atmosphere below 10 Km is fairly transparent to UV, but the ozone concentration, which varies between summer and winter, also suffers shorter terms fluctuations. In the chapter 3, we will see how these ozone concentration varies for two different kinds of geographical zones.

The Troposphere is the layer where the aerosol density is higher. As we will read later, the dust coming from the Sahara Desert may play an important role in the atmos+pheric attenuation problem. It is also characterized by a decrease of temperature with respect to height.

In this layer we also have to pay attention to the volcanic dust. For example, during 1991-1993 it was detected in La Palma Observatory an increase of 0.1 magnitudes in extinction (a different of 10% in the atmospheric transmittance), calculated in the V band, due to dust ejected into atmosphere by the eruption of Mt. Pinatubo in the Philippines [23].

In this simulation, we have not studied the water vapor absorption because it is only important for wavelength higher than 800 nm (Cherenkov wavelength range goes from 280 nm to 300 nm). Also, the O_2 absorption bands are located in wavelength lower than 260 nm, and there is one absorption band at 700 nm, but they are not important [22].

In order to study the extinction of EAS at different zenith angles we have to study the three main processes that can affect to the attenuation of Cherenkov light at ground level.

- *Rayleigh scattering* is due to molecules and its effects is more important for the shorter wavelength.
- *Mie scattering* is due to the dust suspended in the atmosphere, its effect is higher at low heights.
- *Ozone absorption* is very important between 290 to 340 nm and for low energy shower in which most of the light emission occurs at heights where the amount of ozone is high.

1.4.1 Air mass factor

One of the simplest way to describe the atmosphere is to suposse that it is a plane-parallel atmosphere, instead of spherical one. With a plane-parallel atmosphere, we can use the factor $\sec z$ (where z is the zenith angle) to describe the atmospheric ray path for different zenith angles. But, as we will see later this factor is only valid for low inclinations (up to a zenith angle of 60°). We are interested in EAS with zenith angles higher than 60°, so we cannot use the ($\sec z$) to calculate the air mass crossed by an EAS. We have to use a better approximation taken into account the atmospheric curvature. By geometrical considerations, we can calculate the different atmospheric path between a vertical shower and a shower with a zenith angle z, and we obtain the following formula for the air mass.

$$m(z, H_v) = \frac{\sqrt{R_e^2 \cdot \cos^2 z + 2 \cdot R_e \cdot H_v + H_v^2} - R_e \cdot \cos z}{H_v} \tag{1.23}$$

where, R_e is the earth radio, z is the zenith angle and H_v is the vertical height below the ray path. For $\frac{H_v}{R} \to 0 \quad \Rightarrow \to \sec(z)$ as we shown in the figure 1.8.

We can compare the difference between the ($\sec z$) and m(z) in the Fig. 1.8. As we can see in this plot for a value of the zenith angle equal to 70°, the difference between these two formulas is 5%; for zenith angles around 80° the difference between these two quantities is about 20%. If we increase the zenith angle to 85° the difference goes up to 40°.

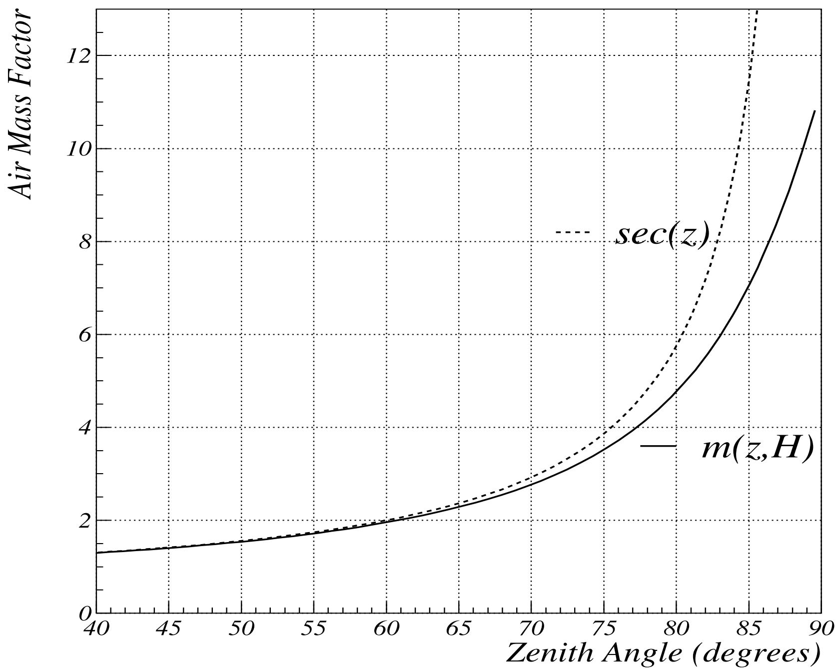

Figure 1.8: *Air mass comparison between the* $\sec(z)$ *and* $m(z)$*. To compute the plots we have considered the earth radio as 6348 Km. and* H_v *equal to 100 Km, to ilustrate the effect.*

The equation (1.23), is valid for almost all the angles but, if we want to make observations with zenith angles higher than 80°, we could have problems with the deflection of the Cherenkov light due to the refraction in the atmosphere. This problem could be important for the low energy air showers and for high zenith angles, because the Cherenkov radiation has to travel a long path inside the Atmosphere.

In the case of the Thickness transversed, the air mass factor is not valid above 80°, to reproduce the atmospheric depth at different zenith angles. Now we had to use the following formula that express in a better way the atmospheric thickness for different zenith angles.

$$AM(z,R) = \sqrt{\frac{\pi R}{2H}} \cdot exp\left(\frac{R\cos^2 z}{2H}\right) \cdot erfc\left(\frac{R\cos^2 z}{2H}\right) \tag{1.24}$$

where R is the radius from the center, and H is the scale Height.

In the table 1.1, we show the difference in the optical path ray obteined with and in the atmospheric thickness for several zenith angles. We also compare those values with the values obtained with the factor $\sec z$.

Zenith Angle	**path length with m(z) factor [Km]**	**path length with** $\sec z$ **factor [Km]**
0°	113	113
20°	120	120
30°	130	130
40°	147	150
50°	174	176
60°	220	226
70°	311	330
80°	529	650
85°	770	1300
89°	1098	6463
90°	1204	∞

Table 1.1: *Increase of optical ray path with zenith angle as seen at El Roque de los Muchachos Observatory level.*

There is difference in the path length above 70° is clear. Moreover, the value obtained for 90° is completely wrong, because the atmospheric size is not infinite!!.

Zenith Angle	**Atmospheric Thickness AM(z)** (gr/cm^2)	**Atmospheric Thickness m(z)** (gr/cm^2)	**Atmospheric Thickness** $\sec(z)$ (gr/cm^2)
0°	793	793	793
20°	843	844	844
30°	914	915	916
40°	1033	1035	1035
50°	1230	1233	1235
60°	1579	1584	1586
70°	2300	2309	2320
80°	4410	4480	4600
85°	8100	8500	9100
89°	20215	23070	45440
90°	29120	32860	∞

Table 1.2: *Increase of atmospheric thickness with zenith angle as seen at El Roque de los Muchachos Observatory level.*

Chapter 2

Attenuation in EAS at HZA

2.1 Introduction

When we have EAS at HZA we know that this EAS has to travel a large amount of atmosphere, so all the attenuation processes will be more important for HZA than for low zenith angle showers and we have to simulate the atmosphere in a detailed way.

These attenuation processes, as we will see below, depend on: *the energy of the primary particle*. If we have a high energy shower the maximum production of photons is going to take place when the beam has crossed a big part of the atmosphere and in this case the ozone is not very effective. The other important effect is the air mass transversed by the HZA showers. In this kind of showers the air mass crossed by the beam is higher and the attenuation of the Rayleigh and aerosol scattering increases. As before, about the problem of the energetic showers and where (in the atmosphere) it reaches the maximum photon production.

We have used the model described in [24], the so called Elterman's model, to calculate the Atmospheric transmission for the Mie scattering and Ozone absorption. We have also used results obtained from the book *Radiation in the atmosphere* [27] for the Rayleigh scattering.

Elterman's model is based upon the *U.S. Standard Atmosphere, 1962*, plus an aerosol content that is characteristic of a meteorological range of about 25 Km. above the sea level. The deviation of the model is based on a turbid atmosphere that is a molecular atmosphere plus aerosol and ozone components.

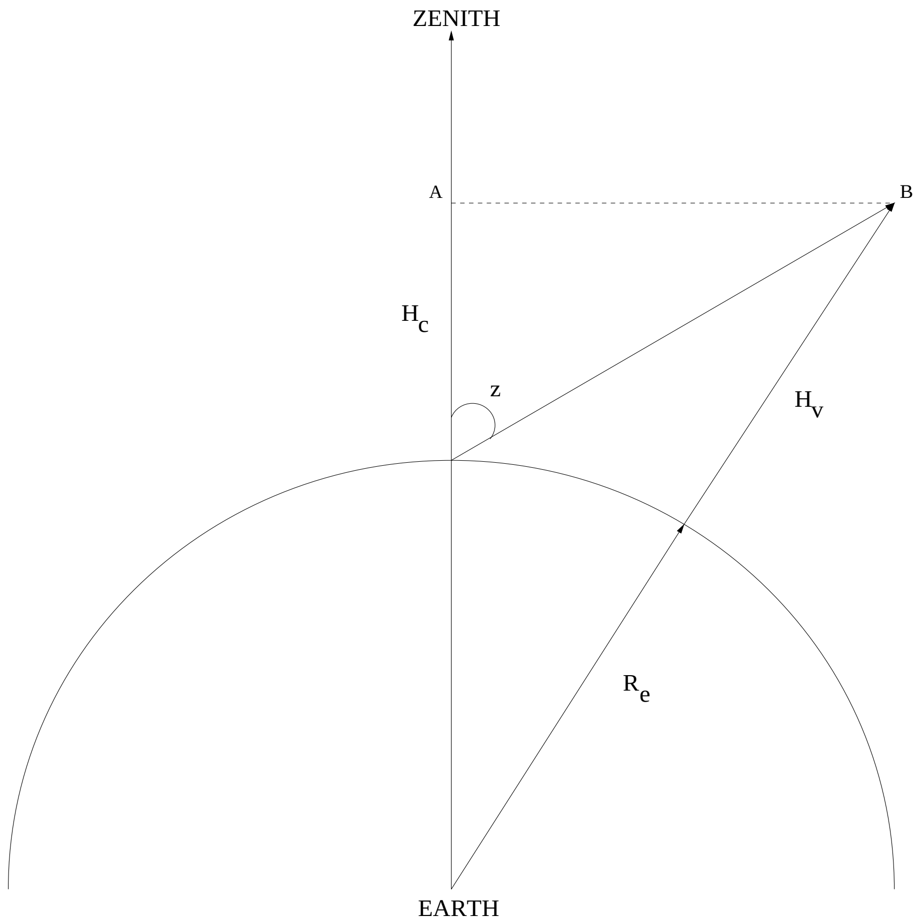

Figure 2.1: *Coordinate change for showers with high zenith angles.*

The transmission coefficient between two altitudes has been calculated with the following expression:

$$T_{tot} \quad = \quad T_{ray} \cdot T_{Mie} \cdot T_{Ozo} \quad = \quad e^{(\tau_{tot} \cdot m(z))} \tag{2.1}$$

where m(z) is the air mass crossed by the cascade, and τ is the optical thickness.

$$\tau_{tot} \quad = \quad \tau_{Ray} + \tau_{Mie} + \tau_{Ozo} \tag{2.2}$$

$$\tau_{Mie} + \tau_{Ozo} \quad = \quad \sum_{2Km}^{h} \beta_{Mie}(h)\Delta h \quad + \quad \sum_{2Km}^{h} \beta_{Ozo}(h)\Delta h \tag{2.3}$$

For the aerosol scattering and the ozone absorption we have used the attenuation coefficients (β_{Mie} and β_{Ozo} in Km^{-1}) per kilometer between 2 and 50 Km and for the wavelength: 280, 300, 320, 340, 360, 380, 380, 400, 450, 500, 550, 600, 650 nm.

For each wavelength we have tabulated the optical thickness between 2 Km (observation level) and a height h (where h goes from 3 Km to 50 Km). In this way, if we want to know the atmospheric transmittance at a fixed wavelength and at a fixed height we only have to go to our optical thickness table, interpolate the value of the optical thickness for our height and get the value, then we have to multiply for the air mass factor. With these two values we can calculate the atmospheric transmission coefficient.

2.2 Rayleigh Scattering

The Rayleigh scattering does not destroy the photons but scatters them. However the differential scattering cross section is rather flat, approximately $[1 + \cos^2\theta]$ (where θ is the angle between the incident photon and the scattered photon), so for our very small angular aperture, to be collected by our detectors, in the EAS, most scattered photons are lost. Rayleigh scattering is proportional to $\frac{\rho}{\lambda^4}$, where ρ is the local air density and λ is the wavelength of the scattered light.

To estimate the amount of Cherenkov light scattered out of the Cherenkov beam accompanying the extensive air shower towards the ground at angle z, we have used different atmospheric densities for different layers in the atmosphere. The equation for the Rayleigh transmission has been obtained from [11], but we have considered a plane-parallel atmosphere.

$$T_{Ray} = e^{-\left[\frac{(X_{down}-X_{up})}{X_{Ray}}\left(\frac{400nm}{\lambda}\right)^4\right]} \tag{2.4}$$

where, X_{Ray} is the mean free path for scattering at $\lambda = 400nm$ and X_{down} and X_{up} are the atmospheric depth.

$$X(z,h) = \int_a^b \rho(H)ds \simeq m(z)\int_a^b \rho(H)dH \tag{2.5}$$

$X(z, h)$ is the atmospheric thickness between our observation level and a vertical height h. The approximation in the equation 2.5 is crucial for the develop of our studies in the longitudinal development of EAS.

To calculate the atmospheric density for each point at high zenith angles, we have to make a change in coordinates. Our simulation code works with a plane-parallel atmosphere and the density is calculated with the vertical height H_c (See fig. 1). If we want to study extensive air showers with high zenith angles, the density at a point A must be calculated with the height H_v. In our simulation code we receive the height H_c as an output value, then we calculate the new vertical height with the equation 2.6 and compute the density for the point A with the new height H_v.

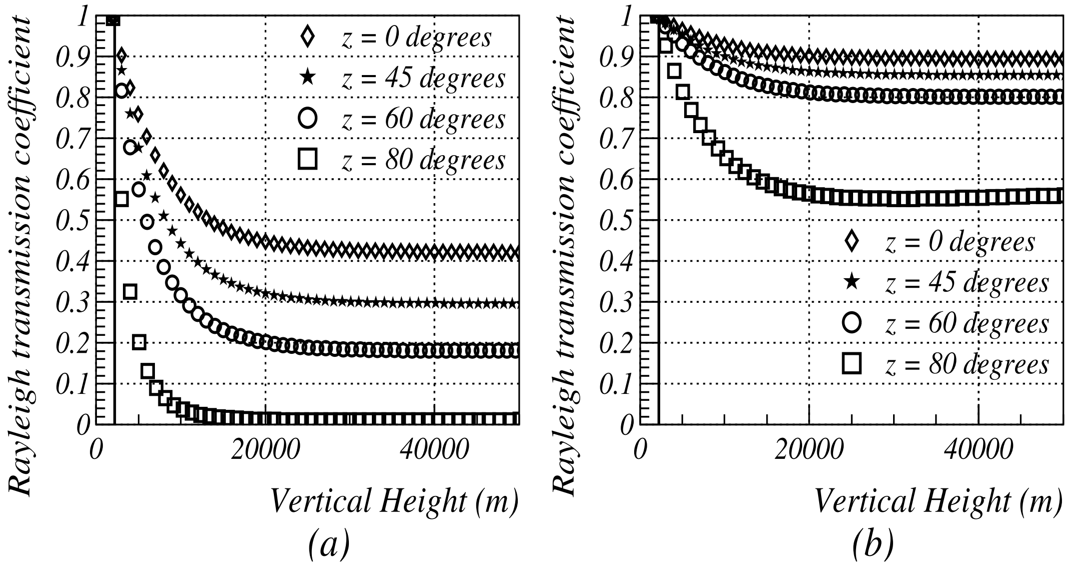

Figure 2.2: *(a) Rayleigh Transmission coefficient for a wavelength of 300 nm at different zenith angles. (b) Rayleigh Transmission coefficient for a wavelength of 500 nm at different zenith angles. The solid vertical line correspond to El Roque de los Muchachos Observatory altitude.*

In this way we calculate the new vertical height in each position for each angle, (this method is used to compute the aerosol scattering and the ozone absorption as well). When we have the value of the density at the point A with the new height H_v, we calculate the atmospheric depth X_{up}. In our simulation X_{down} is the atmospheric depth at El Roque de los Muchachos Observatory height (2200 m a.s.l.).

$$H_v = -R_T + \sqrt{R_T^2 + \left(\frac{H_c}{\cos z}\right)^2 + 2 \cdot R_T * H_c} \tag{2.6}$$

Taking into account all these features we have obtained the results shown in figure 2.2. We have plotted the Rayleigh atmospheric transmission for two different wavelengths (300 nm and 500 nm). The absorption is bigger for shorter wavelength, as expected due to the λ^{-4} law. It can be seen too the decrease in the transmission when we go to larger zenith angles. This effect is also due to the air mass crossed by the shower and therefore the possibility of scattering with a molecule is larger.

The atmospheric transmission for heights near the observation level increase because the distance that a photon, generated at this height, has to travel is shorter, and the chance of this photon to be scattered in this path decrease. Moreover, the difference in the atmospheric depth for these heights and the observation place is small, and the photons generated when the beam is near the observation level have a higher possibility to reach the ground. This is the reason of the high transmisivity we have when the shower is close to the ground.

2.3 Mie Scattering

Dust suspended in the atmosphere scatters incoming light due to its small particles (aerosols) that its size is comparable to the wavelength of light. With this attenuation effect we have an additional problem because El Roque de los Muchachos Observatory is near the Sahara desert (the distance between La Palma island and Africa is 400 Km.). In winter, the desert aerosols are transported across the Atlantic towards the northeastern coast of South America. In summer, the Sahara depression and the semi permanent ridge over Libya act in concert to transport dust over the western and this dust reaches the Canary Island (in these months, the dust can reach even the Caribbean Sea) [29],[30].

Seasonal maps of the desert dust optical depth (at a wavelength of 550 nm) over the Atlantic Ocean, obtained by the Meteosat satellite between 1984 to 1994 show that there is a change in the atmospheric transmission over the Canary

Island, due to aerosols that vary from 95% in winter months to a 74% in the summer [29]. Obviously, we have to know the aerosol amount with respect to the height in the Canary Islands (or the aerosol optical depth). With these measurements we could calculate the atmospheric transmission for aerosols for each height.

Elterman's model considers that the size distribution of aerosols do not change with the altitude. This would be a problem for our study because when the aerosol radio increase, the scattered angle decreases (for a fixed wavelength). Nevertheless a sample of dust collected from El Roque de los Muchachos Observatory showed that the sizes of the particles was very uniform, in the range 20 μm to 60 μm [31].

We have used the values of the aerosol attenuation coefficient given in the Elterman's model per each kilometer up to 30 km, and compute the optical depth for each height and for each wavelength The maximum aerosol density is located near the ground level, when go up in the atmosphere the aerosol density decreases up to 10 km, then the density increases up to 20 km. Taken into account these features, we can say that Elterman atmospheric model could be considered as low aerosol concentration model but, as we will read later, for most of the nights, this would be considered as a good model for La Palma sky.

In the figure 2.3, we show the aerosol transmission coefficient for two different wavelength and for different zenith angles. We can see that the atmospheric transmission is almost the same for different wavelengths and for the same zenith angle. It can be explained taking into account that the aerosol attenuation follows an empirical relation where the wavelength goes as $\lambda^{-\alpha}$ [30] (remember that Rayleigh scattering follows a λ^{-4} relation, so the absorption is bigger for shorter wavelength than for larger) and α is a parameter that has to be determined from linear fits on log-log plots of the aerosol extinction versus wavelength. This parameter depends on the observation place and seasons. As a general rule, the α parameter varies from 0 to 1. Typical continental aerosols (at sea level) have $\alpha = 1$ and typical arid region aerosols have α approximately equal to 0.

Measurements taken in La Palma in June 1984 from Sahara dust showed a wavelength exponent of $\alpha < 0.002$ for the range $350nm < \lambda < 550nm$ [30]. Then, with this α value, we can consider La Palma as an *arid region* for most of the nights of the year. But during the summer when Sahara dust reaches La Palma and we have the so called *"calima"*, we cannot consider El Roque de los Muchachos observatory as an *arid region*, the scattering due to aerosol is the most important atmospheric effect. Obviously, if we have not got better measurements for optical thickness during the summer, we can not give correct values of the aerosol atmospheric scattering during these days when the *"calima"*

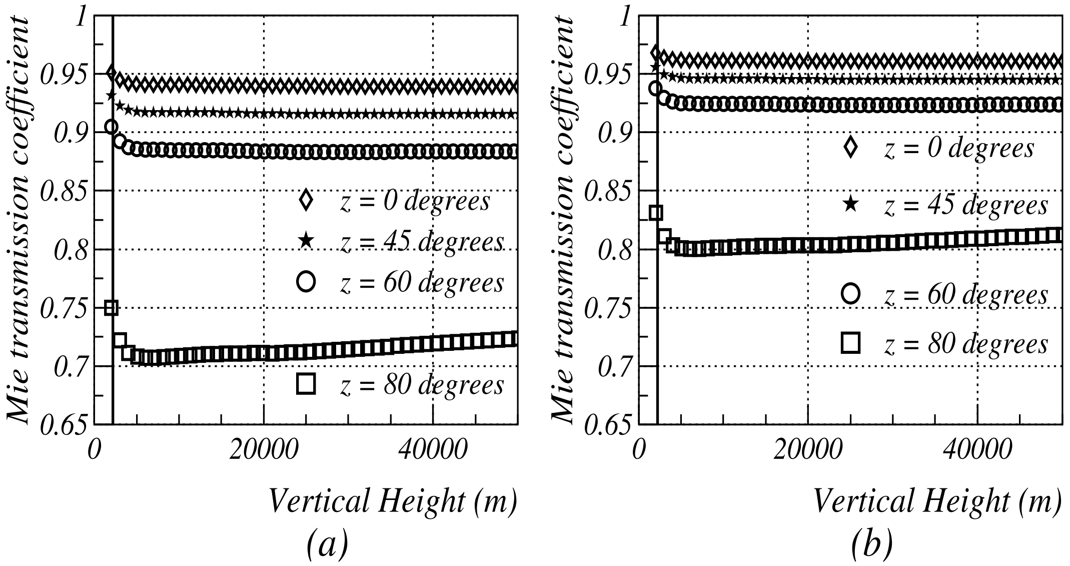

Figure 2.3: *(a) Mie Transmission coefficient for a wavelength of 300 nm at different zenith angles and (b) Mie Transmission coefficient for a wavelength of 500 nm at different zenith angles. The solid vertical line correspond to El Roque de los Muchachos Observatory altitude.*

is so important. Due to its variability these measurements are difficult to be done.

For a fixed wavelegnth and fixed zenith angles, the Mie transmission coefficent is the almost the same except for 80°. Moreover, the transmission coeffcient don't change with respect to the altitude.

We can say too that Elterman's aerosol model is a good approximation for a place with low aerosol content, like La Palma during the winter, spring, fall and almost all the nights during the summer, so this model can be used for our calculations. But, in the summer nights when the *"calima"* appears, there is a high aerosol content and this model should not be used.

2.4 Ozone Absorption

The Ozone is concentrated in a layer between 12 and 30 Km height. In the wavelength range under study we have the very intensive absorption band, called the Hartley band, extending from about 220 to 320 nm (with the maximum absorption wavelength at 243 nm). The neighboring band, the so called Huggins band, is the region 300 to 345 nm. In the visible region a less intensive absorption band is present; the Chappuis band (440 to 750 nm). Its effect is negligible in comparison with the other two bands [27]. The Hartley and Huggins bands are responsible for the absorption of almost all radiation between 280 nm to 340 nm.

The atmospheric transmission coefficient due to ozone is difficult to calculate (like the aerosol transmission coefficient) because of the amount of ozone in the stratosphere varies with respect to the season. Moreover the amount of ozone varies with respect of the latitude. Due to this effect we have calculated the transmission coefficient of the ozone in two different ways. First, we used the ozone concentration from the Elterman's atmospheric model and we obtained the transmission coefficient of the ozone in the atmosphere as in the case of the aerosol scattering. Secondly, we took the equation 2.7 used in astrophysics to calculate the extinction of star's flux in magnitudes per air mass [25], and we calculated the absorption coefficient with this new method.

$$A_{Ozo}(H_v, \lambda) = 1.11 \cdot T(H_v) \cdot k(\lambda) \tag{2.7}$$

where, $k(\lambda)$ is the absorption coefficient in cm^{-1}, and $T(H_v)$ is the total ozone concentration for a typical Tropical region, above the vertical in each position in $atm \cdot cm$ [1] from [28] being tabulated as a function of the height and season. The coefficient 1.11 was chosen to correspond to Eleterman's optical thickness for ozone at 320 nm.

Now we want to know which is the extinction in magnitudes per air mass between two heights H_{v1} and H_{v2} (where H_{v1} is higher than H_{v2}), then

$$A_{Ozo}(H_{v2}, \lambda) - A_{Ozo}(H_{v1}, \lambda) = 1.11 \cdot k(\lambda)[T(H_{v2}) - T(H_{v1})] \tag{2.8}$$

[1] 1 $atm \cdot cm$ of gas $= \frac{M}{2.24 \cdot 10^4} \frac{g}{cm^2}$, where M is the molecular weight of the gas, and 1 $(atm \cdot cm)_{STP} = 2.69 \cdot 10^{19} \frac{molecules}{cm^2}$, where STP is the Standard Temperature and Pressure.

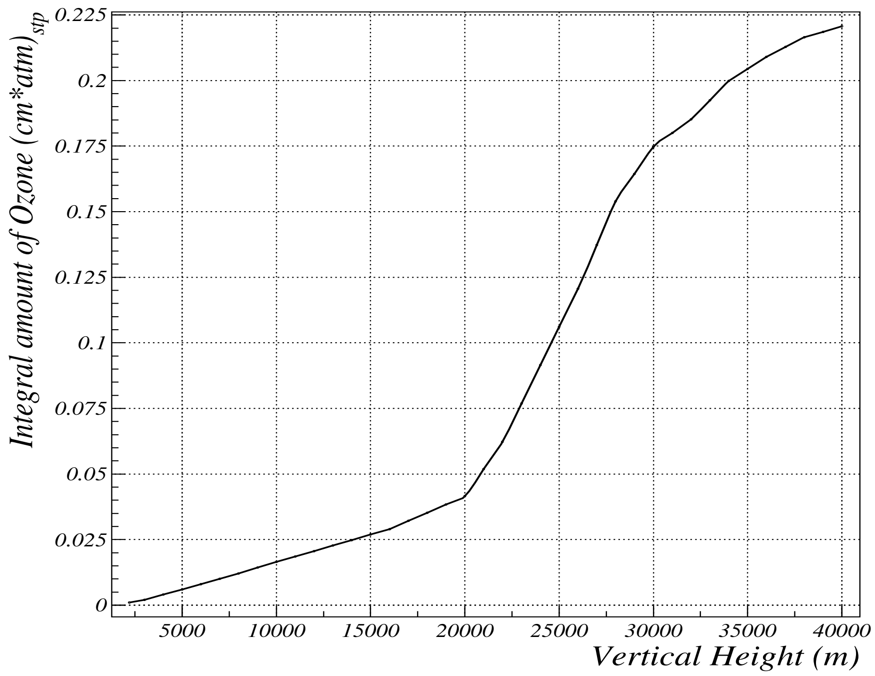

Figure 2.4: *Amount of ozone between 2 Km. and 40 Km for a typical Tropical region.*

$$\Delta A_{Ozo}(\Delta H, \lambda) = A_{Ozo}(H_{v2}, \lambda) - A_{Ozo}(H_{v1}, \lambda) \tag{2.9}$$

where, $(T(H_{v2}) - T(H_{v1})$ is the amount of ozone from El Roque de los muchachos Observatory to the height H_{v1}. These quantities are tabulated for a *Tropical atmosphere*, can be see these values in the fig. 2.5. We note that beyond 40 Km, the amount of ozone is the same for both models, because all of the ozone is located between 20 and 30 Km.

Using the Pogson law [2] we can determine the transmission coefficient and we have the expression

$$T_{Ozo} = 10^{-0.4 \cdot \Delta A_{Ozo}(H_v, \lambda) \cdot m(H_v, z)} \tag{2.10}$$

[2]The Pogson law is a relation between the radiation flux of a star that reach the ground level and the radiation flux of a star outside the atmosphere, in magnitudes units. $m_{in} - m_{out} = -2.5 \cdot \log\left(\frac{I_{in}}{I_{out}}\right) = -2.5 \cdot \log k_t$ where k_t is the transmission coefficient.

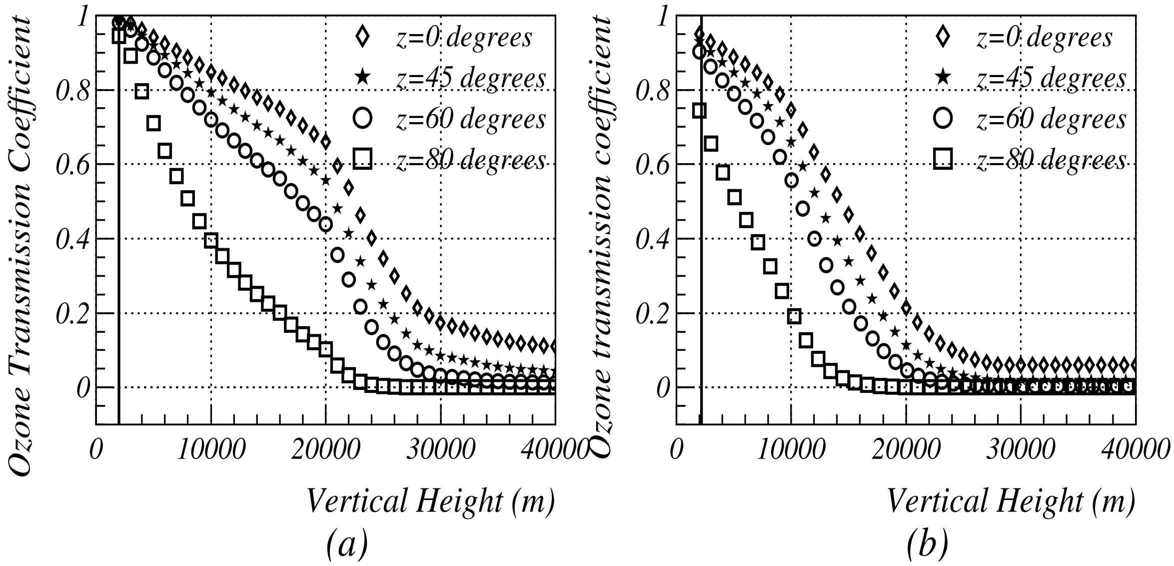

Figure 2.5: *(a) Tropical ozone Transmission coefficient for a wavelength of 300 nm at different zenith angles and (b) Elterman ozone Transmission coefficient for a wavelength of 300 nm at different zenith angles. The solid vertical line corresponds to El Roque de los Muchachos Observatory altitude*

With these two values of the ozone transmission coefficient, obtained from the Elterman's ozone model and the tropical ozone model, we can prove that in both cases the absorption of radiation is very high for short wavelength. The two results are not equal. We did not expect that the two transmission were equal, because the amount of ozone was different for Elterman model and for Tropical model.

As we can see in the figure 2.5, the transmission coefficient for the ozone decreases as the zenith angle increases. This effect occurs because the air mass crossed by the beam increases when the zenith angle increases, as we said before.

2.5 Total attenuation

Finally, we check which is the effect of these three processes together. Once again we plot the atmospheric transmission for two different wavelengths and for four different zenith angles (see figure 2.6).

For shorter wavelengths we have a complete attenuation of the radiation for altitudes higher than 10 Km, this extinction is due to the ozone. We must remember that for wavelength longer than 340 nm the ozone absorption may be negligible. Also important for short wavelengths is the effect of the high zenith angle in the transmission coefficient; as we can see for 300 nm and 80° the attenuation is almost total for heights higher than 10 Km. Once again, the atmospheric depth at 80° increases in a factor 6 compared with 0°.

For longer wavelengths the main process that attenuates the radiation is the Rayleigh scattering (remember that the Rayleigh scattering goes with λ^{-4}). The aerosol scattering is not very important because, as we said before, in our model we consider a low aerosol content.

In order to crosscheck our results we compare it with a theorical atmospheric extinction curve at El Roque de los Muchachos Observatory made by the Isaac Newton Group (ING) [3] [26]. They used the Hayes and Latham result [25] to reproduce the atmospheric attenuation, then they calculated some experimental atmospheric attenuation values, and compared this with the theorical curve. They found a good agreement between both results. Now, we are going to check our atmospheric attenuation values with the theorical ones obtained by the Isaac Newton Group.

We calculated the atmospheric transmission for each wavelength and for all the atmosphere, now we did not want to know the atmospheric transmission for the different altitudes, so we integrated the transmission for all altitudes. Then, we changed the atmospheric transmission values for atmospheric extinction values in magnitude values (with the Pogson law), and represent both results.

As we can see our curve has higher values for the atmospheric extinction than the ING curve, the difference is about 0.03 magnitudes for longer wavelength and

[3] The ING institution controls three of the optical telescopes situated in *El Roque de los muchachos* Observatory at La Palma island. These telescope are: William Herschel Telescope, Jacobus Kapteyn Telescope, Issac Newton Telescope.

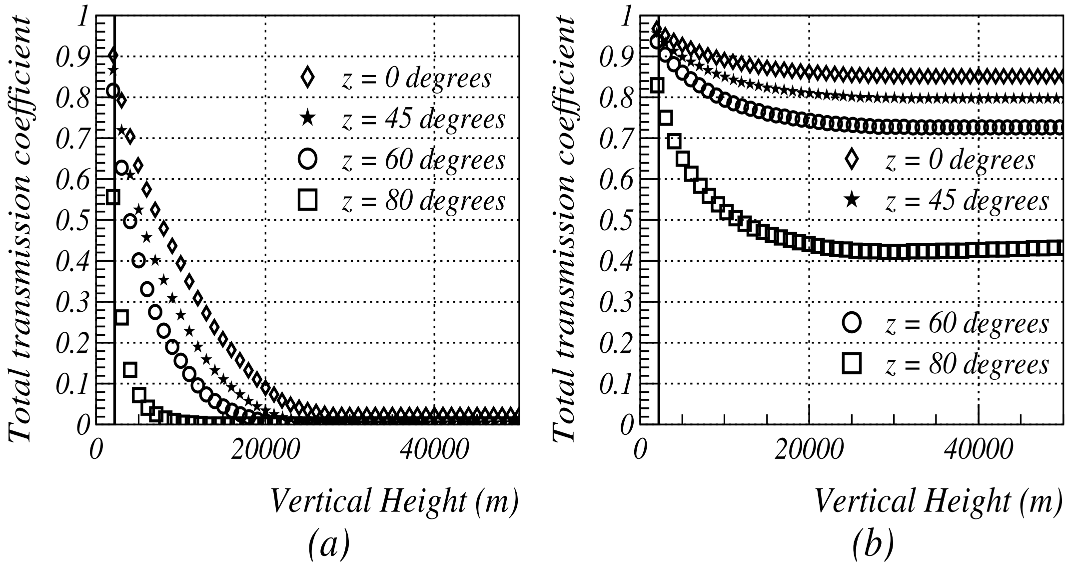

Figure 2.6: *(a) Total Transmission coefficient for a wavelength of 300 nm at different zenith angles and (b) total Transmission coefficient for a wavelength of 500 nm at different zenith angles. The solid vertical line corresponds to El Roque de los Muchachos Observatory altitude.*

higher for shorter wavelength. The difference in the shorter wavelength is due to the ozone concentration in the atmosphere. The Isaac Newton Group used a low ozone density atmosphere (they took the ozone amount from the Allen book [22] and in our model we used an atmosphere with more ozone density.

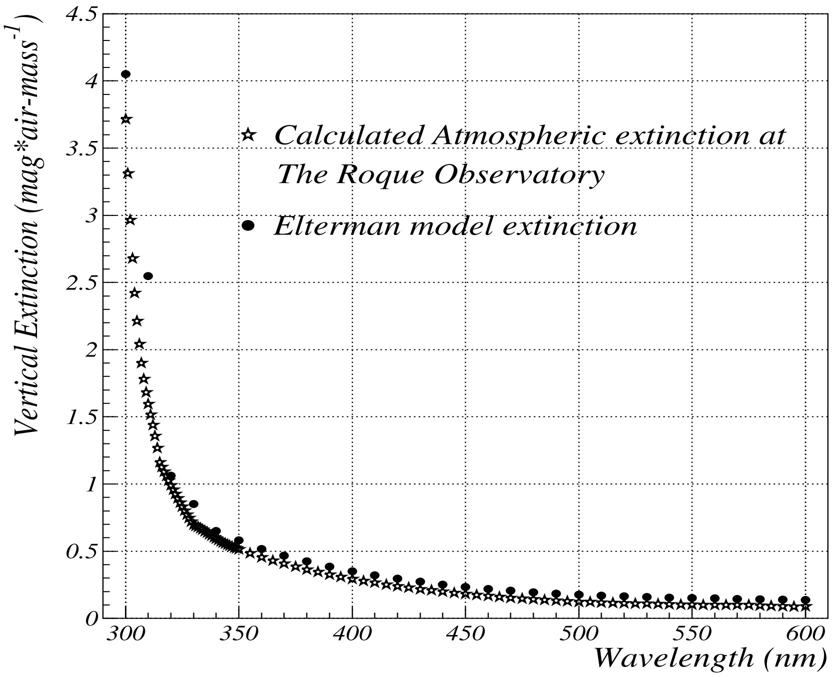

Figure 2.7: *Comparison between the Isaac Newton Group (ING) theorical extinction curve and our theorical extinction curve.*

Chapter 3

Simulation of Extensive Air Showers at High Zenith Angles

3.1 Introduction

Cherenkov detector operating at High Zenith Angles can become a powerful telescope at very high γ-ray astronomy due to the increase of the effective collection area. Moreover the observations at high zenith angles allow to extend the observations time window for any object seen at small zenith angles, as well as to enlarge the dynamic energy range of an instrument towards the highest observable energies of γ-rays [1].

Due to the greatly increased sensitivity at higher threshold energies, this technique enables the study of the high energy end of source spectra which is interesting for various purposes, such as the modeling of the γ-ray emission mechanism at the source, the measurement of the infra-red intergalactic photon density, etc [2].

3.2 High Zenith Angle technique

Ground-based very high energy γ-ray astronomy explores the energy range from 200 GeV up to 20 TeV. The performance of this technique appears to be strongly dependent on the zenith angle range covered while tracking an object. The accessible zenith angle range, for a given object, is simply determined by the latitude of the detector and the celestial coordinates of a particular object. Extension of observations to higher zenith angles might substantially widen the observational time window for a number of objects. In addition observations at large zenith angles favor the detection of the high energy γ-rays, $E \geq 10$ TeV [11] [21], which, at present, can be registered only using the ground-based Cherenkov technique, and set important constrains on γ-ray emission mechanisms.

For HZA observations, the particle cascade in the air-shower develops relatively farther away from the telescope, and therefore, the Cherenkov light from an air-shower is seen through a larger atmospheric depth. This implies a higher detection energy threshold for a trigger based on the photon density at ground level, which leads to a decrease in the observed flux from observed TeV γ-ray sources that exhibit spectra falling sharply with energy. The lower source fluxes are compensated for by the increase in the effective detector area resulting both from the effect of geometrical projection onto the ground and from the shower being more highly developed at the observatory level.

The Cherenkov light is emitted from the air shower near its point of maximum development. For a given primary energy, this corresponds to a certain atmospheric slant depth measured from the top of the atmosphere, so the distance $D(\theta)$ between detector and the point of maximum increases with zenith angle θ. The effective detection area is,

$$A(\theta) = \pi(D(\theta) \cdot \tan\Psi)^2 \tag{3.1}$$

where Ψ is the half-angle of the detector's cone of light acceptance [20]. Exact values of $D(\theta)$ depend on shower energy and the detector's elevation, but very roughly one has $D(60°) \simeq 4 \cdot D(0°)$ and $D(80°) \simeq 20 \cdot D(0°)$. In other words, **a Cherenkov detector's effective detection area is roughly 400 times greater at 80° zenith angle than at 0°**. Note that Ψ should be on the order of the Cherenkov emission angle in air. A larger value of Ψ would increase background acceptance without increasing signal detection. Choosing a small value of Ψ would needlessly reduce the effective detection area.

Of course the Cherenkov light intensity is very much reduced for a shower at a high zenith angle compared with the intensity from an identical shower arriving vertically. If there were no atmospheric attenuation, the Cherenkov light intensity would be approximately proportional to $1/D^2$. Atmospheric attenuation causes a further reduction with zenith angle. Consequently, a detector's threshold energy must be much higher at large zenith angles (being proportional to D^2 if the atmosphere attenuation is ignored).

3.3 CORSIKA code and applied modifications for HZA showers

3.3.1 CORSIKA physics

The standard simulation program used for the simulation of EAS is the CORSIKA program. CORSIKA (COsmic Ray SImulations for KAskade) is a detailed Monte Carlo program to study the evolution of EAS in the atmosphere initiated by photons, protons, nuclei, or any other particle.

The CORSIKA code was originally developed to perform simulations for the KASKADE experiment at Karlsruhe and has been refined over the past years. The development of CORSIKA is guided by the idea to predict not only correct average values of observable with this EAS simulated code, but also to reproduce the correct fluctuations around the average value. In two words, the programme simulates the transport of particles through the atmosphere as well as their interactions with air targets. All particles are tracked along their trajectories.

It is not the aim of this work to give a complete and detailed description of the physics used in CORSIKA ([12]) but to mention the main physical considerations and how CORSIKA deals with them. We will remark the Cherenkov photon production because it is important for this work.

Analyzing experimental data of an EAS requires a detailed theoretical modeling, for comparison, of the cascade processes. This can only be achieved by detailed Monte Carlo calculations taking into account all knowledge of high energy strong and electromagnetic interactions. We have seen in Chapter 1 the main processes that take place in an EAS, so it is easy to see the difficulty in modeling such interactions for all the secondary particles generated in an EAS. Other than this technical problem we have the physical problem that is also rather complicated for two main reasons: there is a big amount of parameters to be taken into account and most crucial is that the knowledge of high energy interactions is still incomplete in important features. The following could be a small list of the main facts that have to be taken into account when simulating an EAS:

- Electromagnetic interactions.
- Hadronic interactions.
- Decay of instable particles, ionization energy loss and deflection by multiple scattering.

- Environmental parameters; mainly the atmosphere.

To finish this small overview of the CORSIKA code we just remark that the major systematic uncertainties in EAS analysis arise from the lack of knowledge of the total cross-section and the details of particle production for nuclear and hadronic reactions at high energies with small momentum transfer. The energetic particles arising from this high energy interactions are of highest importance in the development of EAS, as they are the most energetic secondary particles, which bring the largest energy fraction of each collision deep into the atmosphere. The experimental findings at protons colliders have to be extrapolated, using theoretical models, over many orders of magnitude to CR energies, small emission angles and nuclear projectiles and targets.

3.3.2 Cherenkov Radiation in CORSIKA.

There are some more options in the CORSIKA code that are not going to be discussed in this work. Nevertheless, there is one with important relevance for our work, the Cherenkov photon production in EAS. The Cherenkov light production by electrons, positrons, muons, and charged hadrons is considered in the routines CERENE and CERENH respectively. The Cherenkov photons are considered within a wavelength band and the atmospheric attenuation of the Cherenkov photons is not taken into account, this is the reason why we have made our own atmospheric attenuation simulation program, as you could read in the previous chapter. Because these are the routines that are going to be used for our purpose we will take a closer look at how CORSIKA treats in those routines the generation of such a radiation.

Based on a program extension made by HEGRA collaborators the Cherenkov radiation simulation option is implemented in the CORSIKA code. We have seen in Chapter 1 how and under what conditions this radiation is produced. In the program the condition:

$$\frac{nv}{c} = n \cdot \beta > 1 \tag{3.2}$$

is examined for every transportation step of a charged particle. The refractive index n is approximated by the local density $\rho(h)$ (in g/cm^3):

$$n = 1 + 0.000283 \cdot \left(\frac{\rho(h)}{\rho(0)}\right) \tag{3.3}$$

neglecting the wavelength dependence of n.

The number N_c of photons which are emitted per path length s at an angle θ_c is calculated as:

$$\frac{dN_c}{ds} = 2\pi\alpha \int \frac{\sin^2\theta_c}{\lambda^2} d\lambda \tag{3.4}$$

where the integral extends over the wavelength band, within which the Cherenkov detector is sensitive; α is the fine structure constant, and the angle θ_c relative to the charged particle direction is given by:

$$\theta_c = \mathrm{acos}\frac{1}{\beta \cdot \mathrm{n}} \tag{3.5}$$

The emission of Cherenkov photons is treated in the following way: each charged particle path element is subdivided into smaller fractions such that, within each fractional element, the number of emitted photons is less than a predefined bunch size. This photon bunch is treated as a whole rather than each single Cherenkov photon, thus reducing the computational effort and time considerably. For each photon bunch the azimuthal emission angle is taken at random, and its arrival coordinates at ground level are calculated. As already said, atmospheric absorption of the Cherenkov photons is not taken into account. But by writing the original height of each photon production onto the Cherenkov output file is enough to calculate the attenuation afterwards when we are analyzing the output data.

3.3.3 Applied modifications for HZA showers

CORSIKA code uses a plane-parallel atmosphere to calculate all the particle interactions, so this code is only able to simulate EAS with vertical incidence, that is to say, EAS with a zenith angle of 0 degrees. The atmosphere is divided into five layers, where the atmospheric density changes exponentially. In each of these layers CORSIKA calculate the vertical height of each particle and its respective vertical atmospheric thickness (see fig. 2.1). As we are going to simulate EAS with zenith angle bigger that 0°, we cannot want to proceed in the same way as CORSIKA done. So we have to developed a correcting algorithm.

First of all we choose the zenith angle of the shower and then CORSIKA selects in a random way the height (with respect to the horizontal plane at the detector level) H_c of the first interaction point, namely, the height where the first particle collide with an atmospheric molecule. At this point, we introduce our algorithm. With the zenith angle, and the height of the first interaction point chosen, we calculate the corresponding vertical height (distance along the perpendicular to the ground, from this point to the detector altitude) for this zenith angle H_v (see fig. 2.1). The development of the shower goes downwards and for each vertical height at vertical incidence we calculate its corresponding vertical height at a given zenith angle.

Using this method, we are using a quasi-spherical atmosphere instead of a plane-parallel atmosphere. In each of the points that CORSIKA program evaluate the position of a particle or positron, we change to a local plane parallel atmosphere at this new coordinates.

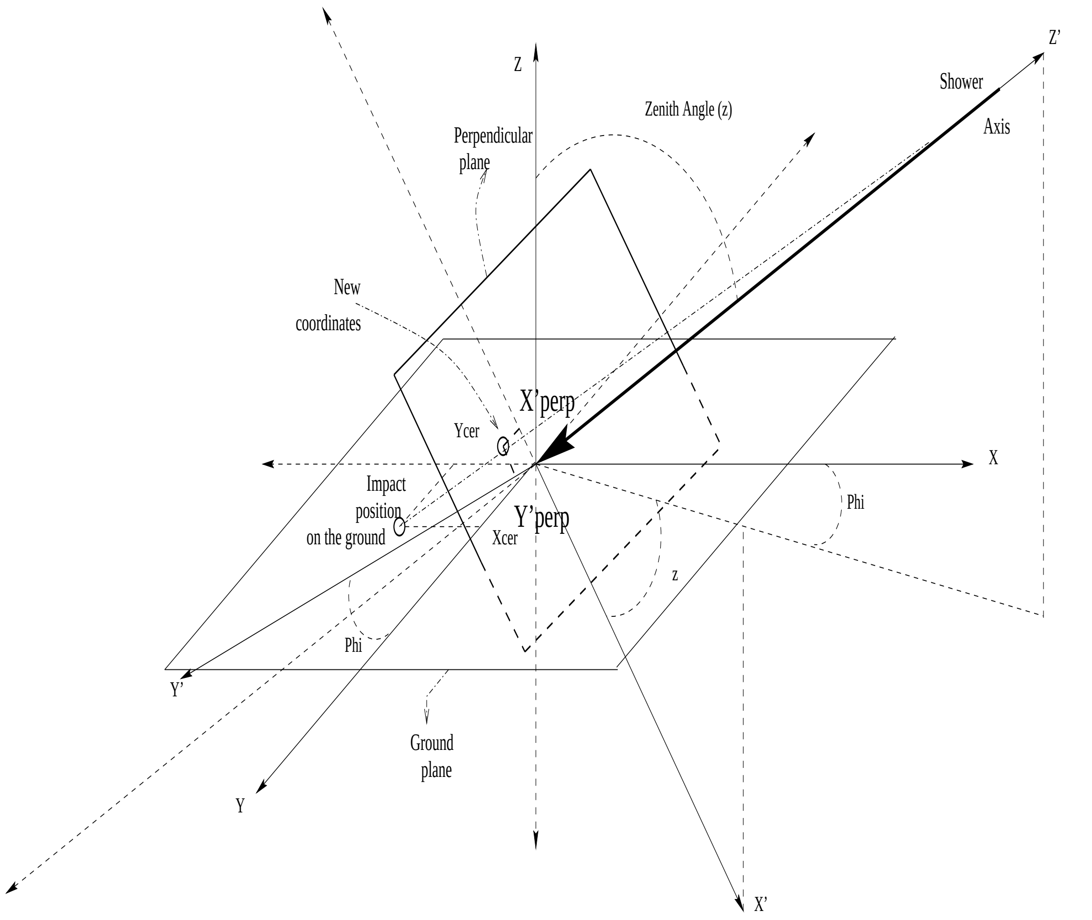

Figure 3.1: *Coordinates system change between Cherenkov photons that reach the ground plane (X_{cer},Y_{cer}), and the Cherenkov photon impact coordinates in the perpendicular plane of shower axis (X'_{PERP},Y'_{PERP}).*

Another item that we had to modify was the way to analyze the Cherenkov photon density at ground level. This quantity is crucial in order to obtain the Cherenkov photon lateral distributions. If we have vertical incident EAS, the perpendicular plane of the shower axis coincide with observation plane in the ground. In this case the lateral distribution of Cherenkov photons is ease to calculate, and the impact coordinates of the Cherenkov photons in the ground are in the correct coordinate system. However, when we are studying EAS arriving with high zenith angles, we have to make a change in the coordinate system of the Cherenkov photons coordinates in the ground. In these cases, the plane perpendicular to the shower axis do not coincide with the observation plane in the ground. The lateral distributions of Cherenkov photons must be computed in the perpendicular plane of shower axis. In EAS with HZA these two planes are not the same and we have to make a coordinate system change. In the figure 3.2, we can see the way we have to make the coordinate change. Once we have the Cherenkov photons coordinates in the correct plane we can calculate the lateral distributions of Cherenkov photons for different zenith angles. In the chapter 4, we will see the behavior of these lateral distributions for different energies.

3.4 γ-EAS development

The study of the Longitudinal distribution for EAS with different zenith angles is very important in the sense that it is a control to know if our modifications applied in the CORSIKA code are correct or not. The longitudinal development of EAS with the same energy in the atmosphere should be similar in terms of thickness , independently of the arriving zenith angle. Of course, now we are not considered the atmospheric attenuation. EAS with HZA suffer more attenuation than EAS with LZA and therefore the longitudinal development is not the same.

It is important to note that, the similarity mentioned above means that γ-ray showers with the same energy will reach the maximum Cherenkov photon production at the same slant thickness. The generation of Cherenkov photons only depend on the amount of thickness crossed and not on the distance transversed [6].

Observing γ-rays under HZA leads to a dramatic growth in the amount of atmosphere traversed by this γ-ray before it arrives to the observer. This effect is shown in figure 3.1. It is worth noting how a correct treatment of curved earth atmosphere leads to a finite thickness of atmosphere at very HZA, as opposite to the infinite thickness obtained by the flat earth model $\sec(\theta)$ (see figure 1.8).

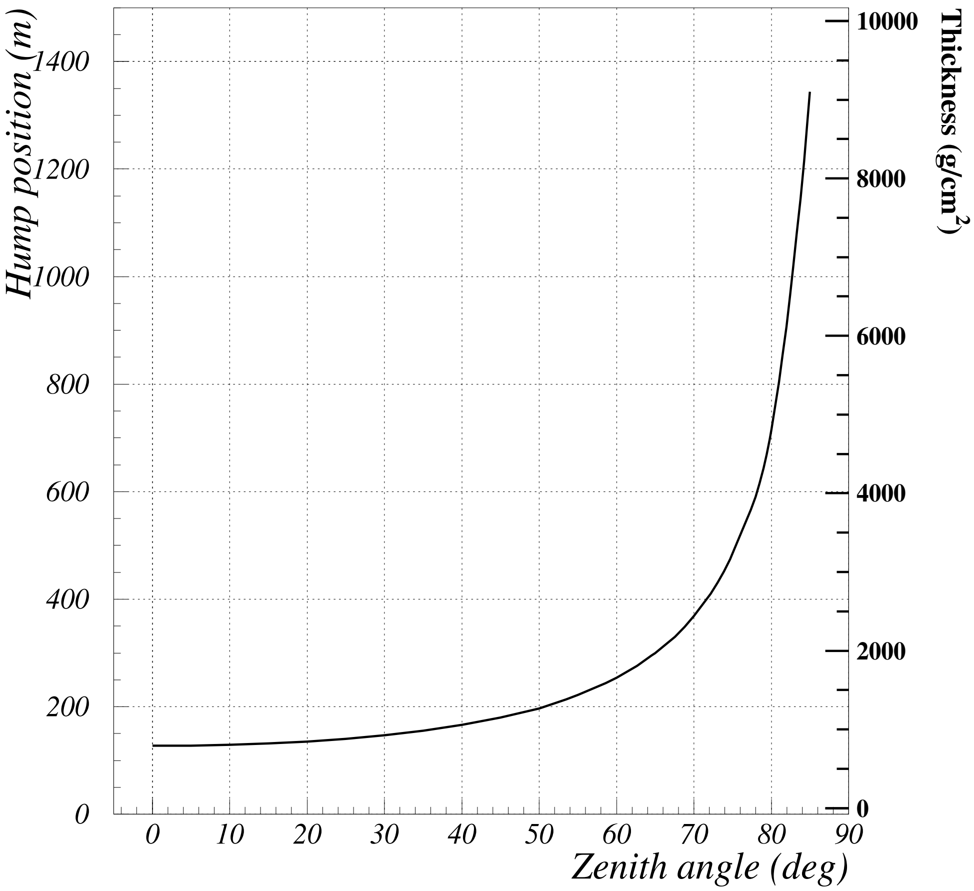

Figure 3.2: *Evolution of thickness (right hand scale) and hump position (left hand scale) with zenith angle. Hump position is calculated using a toy model of a single electron traversing the atmosphere.*

It is also interesting, as we will see later, that the position of the *hump* increase with the zenith angle. This effect is a consequence of the geometrical development of the shower, in the lateral distribution section, we will discuss in more detailed the implications of the displacement of the *hump* position with the zenith angle. Therefore showers viewed under HZA will develop at a larger distance from the observer. Sommers and Elbert, introduces a rough formula to calculate the distance to the shower maximum [20].

$$D = \left[7.1 \ln\left(\frac{1030}{\mathrm{x_{max}}\,\cos\theta}\right) - \mathrm{H}\right] \cdot \sec\theta \tag{3.6}$$

where, H is the detector's altitude, x_{max} is the slant thickness where the showers reach the maximum and θ is the zenith angle.

In the figure 3.1, we can see how the atmospheric thickness increase respect to the zenith angle and the hump's displacement versus zenith angle too. This figure is a simple simulation of a movement of a single electron along the atmosphere. As we will see in the next chapter, this effect of the *hump's* displacement towards large distance from the core, will be presented in our simulations, as we could see in the lateral distributions figures.

In this figure, we have also showed the variation of thickness versus zenith angle. A similar example could be found in the table 1.1 (chapter 1).

In order to compare our results, we have calculated the distance to the shower maximum using our simulations with the aid of the *air-mass factor* (see section 1.4.1). And on the other hand, we have used the Sommers and Elbert's formula (equation 3.1), with the x_{max} obtained in our simulations. In the next table (see table 3.1) we compare both values.

Zenith Angle	**Sommers's formula**	**Our Simulation**
0°	7 Km	9 Km
40°	14 Km	15 Km
60°	27 Km	29 Km
80°	129 Km	113 Km

Table 3.1: *Distance to the shower maximum for 100 GeV γ-showers*

If we compare the results obtained at 80 degrees, we can see that the our simulation result is lower than Sommers's result. The reason for this discrepancy is due to the *air-mass factor*. Sommer s uses the factor *sec* θ , which is known that overestimates the distance for zenith angles higher than 60° [27].

3.4.1 Electrons and positron longitudinal development

The longitudinal profile of the number of secondary electrons and positron in showers of a fixed primary energy, remains almost the same at different shower inclinations when the distance along the shower axis is measured in thickness (gr/cm^2). The depth of the shower maximum can be calculated as,

$$T_{max} = X_0 \cdot \ln\left(\frac{E}{E_c}\right) \tag{3.7}$$

where X_0 and E_c are the radiation length and critical energy in air, respectively [15]. Thus a 100 GeV γ-ray air shower at zenith has, on average, a maximum in electron number at a depth of $T_{max} \simeq 250gr/cm^2$, which, correspond to a $H_{max} \simeq 10km$ above the sea level.

In order to check our modification in the CORSIKA code we simulated showers initializated by γ, with the same input parameter, but with different zenith angles. Under this circumstances, we are interested in the production of the electrons and positrons along the shower. We should have approximately the same longitudinal distribution of electrons and positrons, on average. Once again we are not taking into account the atmospheric attenuation. In the figure number 3.4, you can see what we obtain from our simulation.

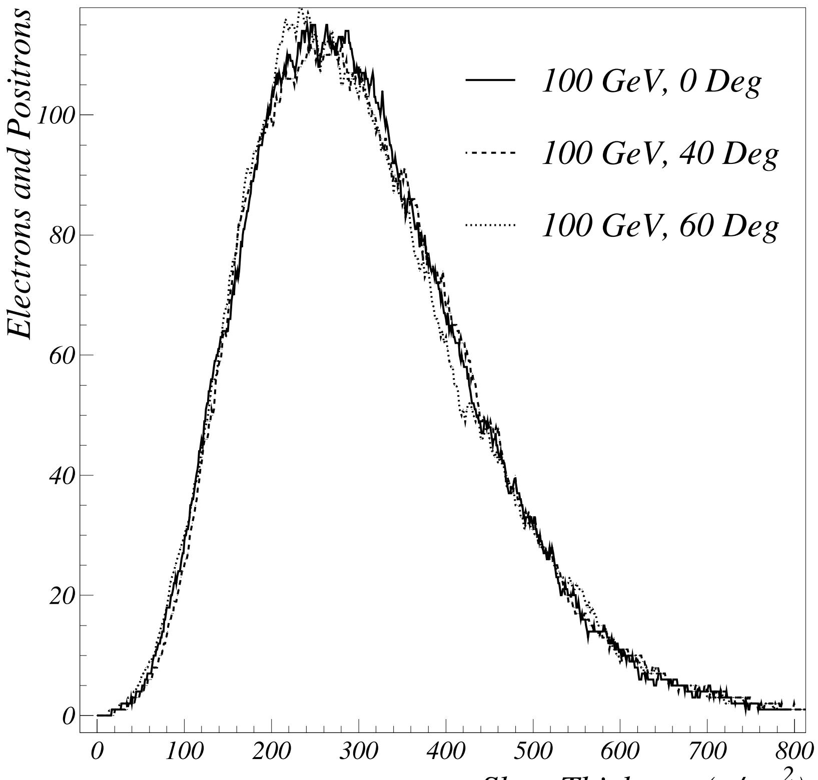

Figure 3.3: *Electron and positron longitudinal development for different zenith angles and for 100 GeV γ initializated showers.*

As we expect, the maximum electron and positron production occurs for the same slant thickness, independently of the zenith angle. In our case, for 100 GeV γ-ray showers, the slant thickness maximum is at 260 gr/cm^2. This means, that our modification produce the same amount of charged particles along the shower's development. We must note that the thickness crossed for HZA showers is bigger that for LZA, so the plane parallel atmosphere is not correct and our quasi-spherical atmosphere correction works in the right way.

3.4.2 Longitudinal development of Cherenkov photons for different zenith angles

As we said before, the longitudinal profile in air showers of a fixed energy remains almost the same for different zenith angles in terms of slant depth. Although, for air showers with large inclinations the total atmospheric optical depth increase substantially and the shower develops completely in the upper layers of the atmosphere. For these showers, the height of shower maximum is far above the observation level, and the geometrical distance from the shower maximum to the observation level is very large. A γ-ray induced air shower of 100 GeV with a 60° of zenith angle, on average has an electron maximum at $H_{max} \simeq 9Km$ in vertical height, is that to say, above the observation level. The corresponding geometrical distance from the shower maximum to observer, S_{max} (see fig. 2.1), for such a shower is about 27 Km. That is in a good agreement with out simulations.

Now we are going to show, how our modification in the CORSIKA programme works properly. For this purpose, we studied two different range of energies. **Low energy showers** (10 GeV and 100 GeV) and **High energy showers** (10 TeV). We will see that for both energies and for all zenith angles up to 80°, the maximum productions of Cherenkov photons are reached at the same slant thickness, as we expect from the result in the electron longitudinal development.

To study Cherenkov photons longitudinal distributions we have simulate γ-ray showers at different zenith angles with our modified CORSIKA program. We have obtained the vertical height and the vertical thickness of each photon and with the aid of the *air-mass factor*, we have calculated the slant thickness of each photon. In order to compare the showers with the same energy, but with different zenith angles, we normalized the total number of Cherenkov photons for each zenith angle point to the one obtained in the zenith angle popint with highest values.

In the figures 3.3 and 3.4 corresponding to low energy showers, we can see how the maximum Cherenkov photon production is the same for all the zenith

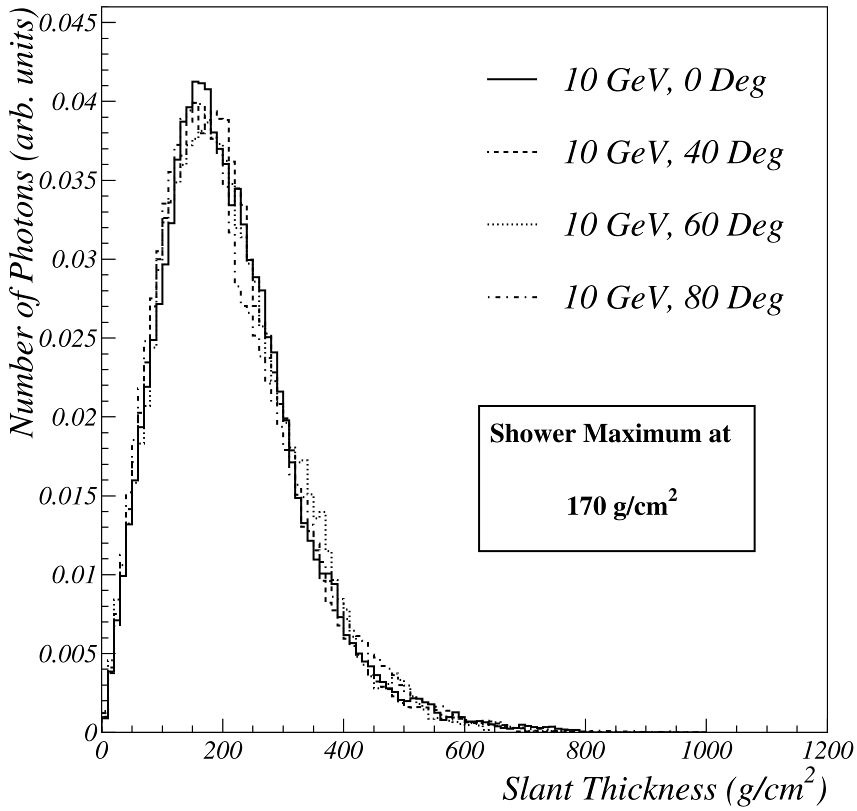

Figure 3.4: *Longitudinal distribution of 10 GeV γ-shower Cherenkov photons as a function of slant thickness for different zenith angles.*

angles, as we expect. In the 10 GeV γ-ray showers these maximum is higher in the atmosphere, reaching a value of 170 gr/cm^2, than in the 100 GeV γ-ray showers. For this energy, the maximum number of photons is 260 gr/cm^2. The difference in the altitude of maximum number of photons is due to the energy of the primary particle. Lower energy showers penetrate less into the atmosphere than high energy showers. This effect is also important for the atmospheric attenuation.

In the case of high energy γ-ray showers we obtain the same result. The maximum shower development is reached at the same slant thickness for all the zenith angles. The value of the maximum production is higher than in the other cases, and it has a value of 420 gr/cm^2. In the figure 3.5 we can also see too that for the showers with an energy of 10 TeV and a zenith angle of 0°, the Cherenkov photons reach the observation level (in our case the position of the

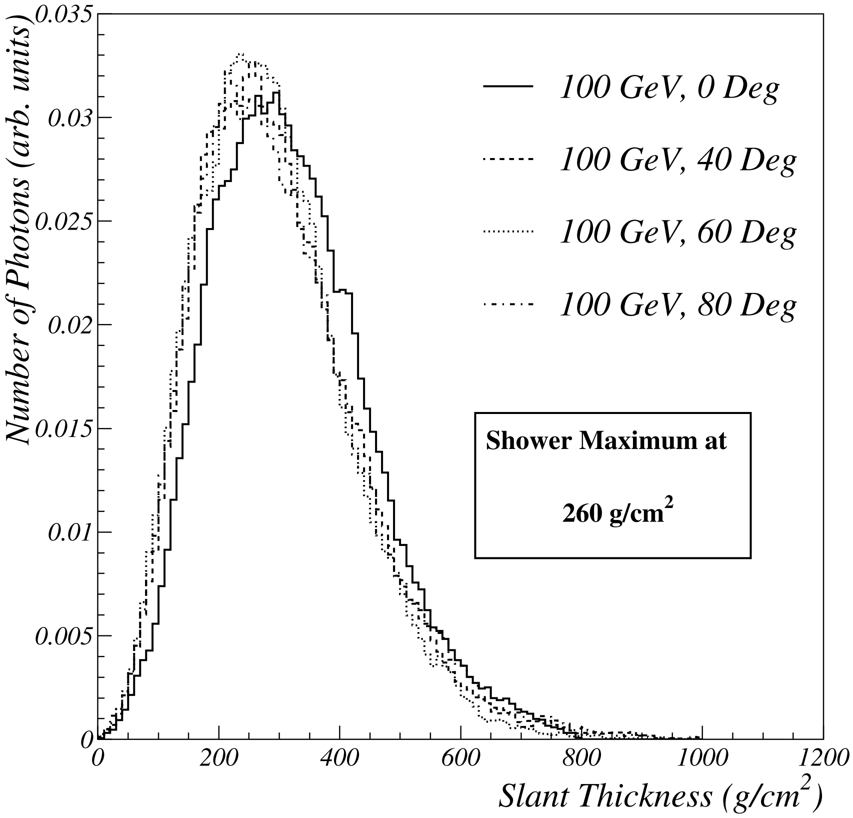

Figure 3.5: *Longitudinal distribution of 100 GeV γ-shower Cherenkov photons as a function of slant thickness for different zenith angles.*

HEGRA experiment in La Palma observatory, at 800 gr/cm^2) before its death.

For very high energies, the Cherenkov photons longitudinal development can reach the ground before it finish. In this cases, our longitudinal profile is stopped at the observation level. This effect is showed in the figure 3.5 for the 10 TeV shower with 0°, the curve finishes at 790 (gr/cm^2) of slant thickness, that is the observation's atmospheric thickness.

These results can confirm that our modification in CORSIKA code works properly in the way that for low energies (in our work we have simulated showers at 10 GeV), and for high energies (in this range we have simulate 10 TeV showers) the longitudinal distributions of Cherenkov photons are the same for the four different zenith angles that we are generated (0°, 45°, 60° and 80°).

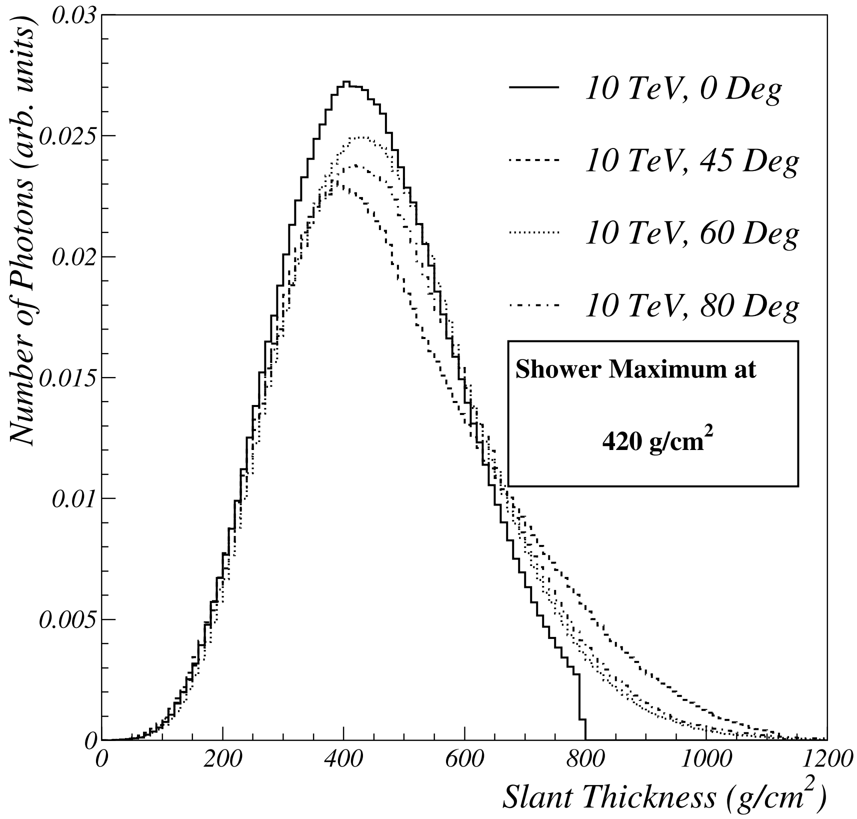

Figure 3.6: *Longitudinal distribution of 10 TeV γ-shower Cherenkov photons as a function of slant thickness for different zenith angles.*

Chapter 4

Results

4.1 Lateral distributions for Extensive Air Showers at High Zenith Angles

The fact that when EAS arrive at high zenith angle, the shower development has to travel a large distance inside the atmosphere, determine the distribution of Cherenkov light in the plane perpendicular to the shower axis. Air showers at low zenith angles give a high Cherenkov photon density in the region close to the shower core ($R \leq 100m$) (see figures 4.1, 4.2, 4.3, 4.4 and curves with zenith angles equals to $0°$, $40°$) because of high photon emission from the low energy electrons ($E_e \leq 1GeV$) which deeply penetrate into the atmosphere and suffer multiple Coulomb scattering.

In EAS with HZA these electrons contribute over a much wider range of distance from the shower core because of the larger geometrical distance to the shower maximum, and as a result the corresponding mean photons density is substantially lower (see figures 4.1, 4.2, 4.3, 4.4 and curves with zenith angles equals to $60°$ and $80°$).

In addition, the absorption of Cherenkov light photons in the atmosphere increases for air showers with large inclinations, as we could read in the chapter 2, due to the large optical depth on the way from the point of their emission to the detector. This effect produce that for γ-ray shower at $60°$ and $80°$ the Cherenkov photon density decrease substantially compare with the low zenith curves.

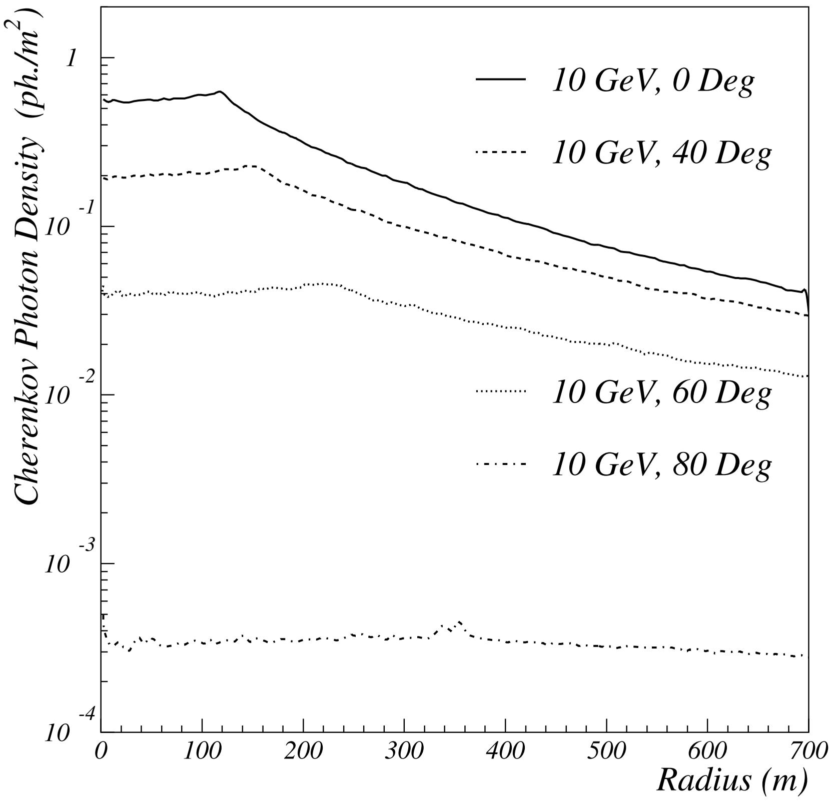

Figure 4.1: *Lateral distribution of Cherenkov light density in 10 GeV γ-ray induced air shower with zenith angles of 0°, 40°, 60°, 80°.*

The characteristic *hump* in the lateral distribution of Cherenkov light photons, caused by the emission of energetic electrons ($E_e \geq 1GeV$) around the shower maximum, is shifted to larger distances from the shower axis. One can estimate the position of the hump using the expression $R_0 \sim S_{max} \cdot \tan\theta_c$, where $\theta_c = \theta_c(H_{max})$ is the Cherenkov light emission angle at the corresponding shower maximum height, H_{max}. Thus for a 100 GeV γ-ray shower at the zenith and for 60° inclination the offset of the *hump* is 110 and 210 m, respectively. These "toy model" estimates are in good agreement with the simulations that we have made, as you can see in the figure 4.2.

In the low energy γ-ray induced showers at 10 GeV and 100 GeV (see figures 4.1 and 4.2), we can see how the lateral distribution density is almost constant up to the *hump* distance. It is also appreciable that for high zenith angles (60°, 80°) the depletion in the Cherenkov photon density is very important. For these

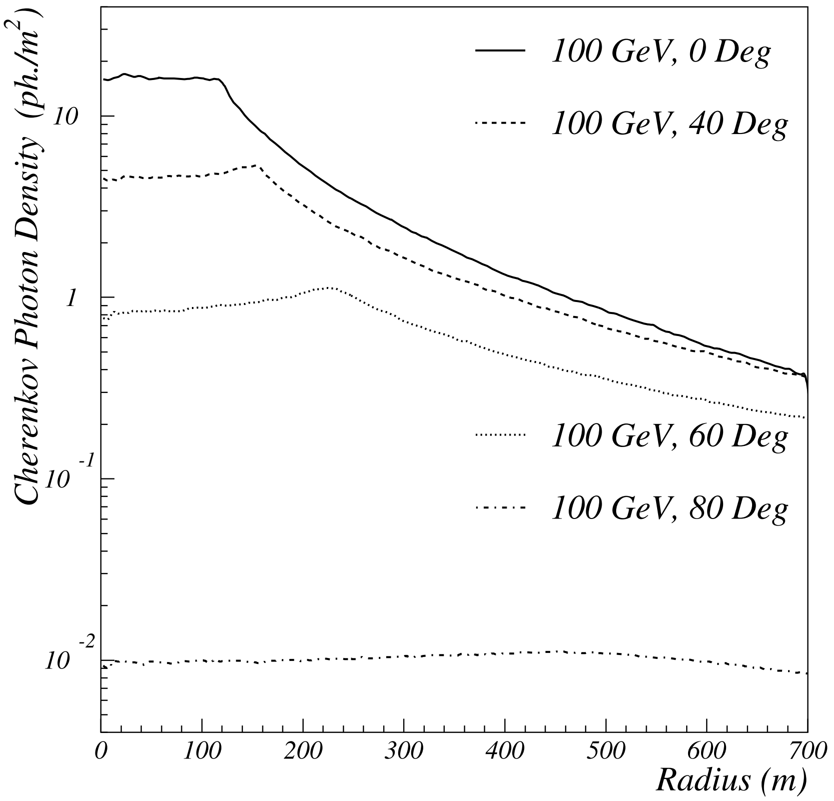

Figure 4.2: *Lateral distribution of Cherenkov light density in 100 GeV γ-ray induced air shower with zenith angles of 0°, 40°, 60°, 80°.*

γ-ray showers the longitudinal development occurs up in the atmosphere and the attenuation is very important.

We have to remark that for HZA showers, the Cherenkov photon density is spread over a big area. Cherenkov light cone reaches the ground after it travels a large fraction of the of the atmosphere. For example, the area covered by the cone for EAS with 80° of zenith angle is over 20 times bigger that the area cover by the Cherenkov light cone for EAS with 0° of zenith angle.

For γ-ray showers with energies of 3TeV and 10 TeV (see figures 4.3 and 4.4), it is easy to observe that the Cherenkov density near the core decrease until the

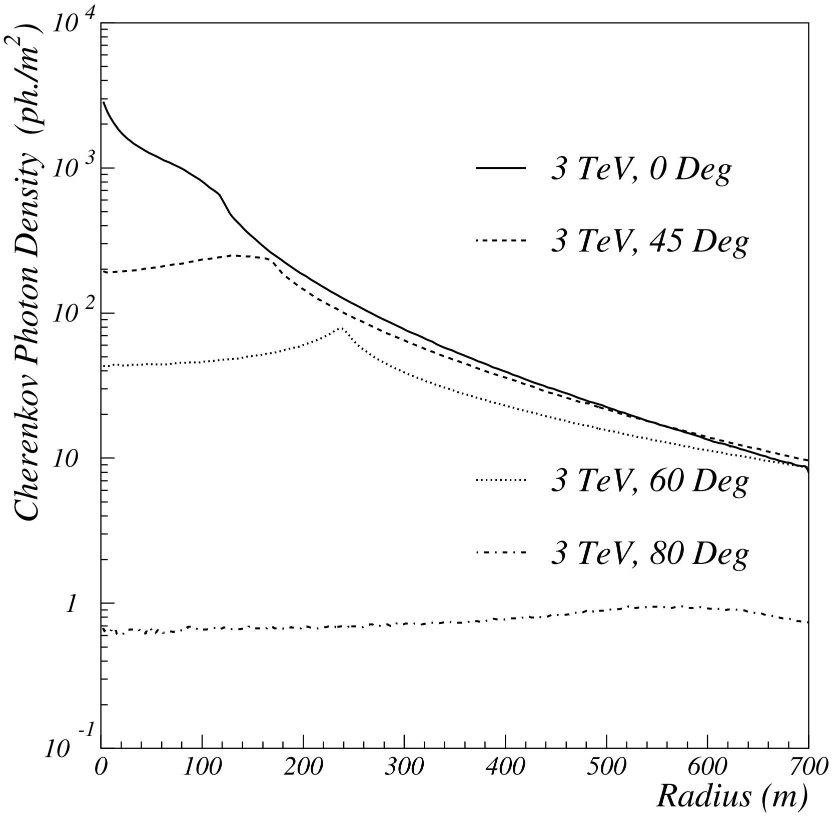

Figure 4.3: *Lateral distribution of Cherenkov light density in 3 TeV γ-ray induced air shower with zenith angles of 0°, 45°, 60°, 80°.*

hump distance for vertical incident showers, but for HZA showers (in our work 60° and 80°) the Cherenkov density increase a little bit until the *hump*. For showers of 60° of inclination, the *hump* is perfectly visible and even for 10 TeV showers, the Cherenkov photons density at the distance of 240 m is equal to the Cherenkov photon density of showers at 0° and 45° on inclination.

For all the energies the *hump's* displacement is the same for each zenith angle. This behavior, is what we expect, because this is a geometrical effect that is independent of the primary energy of the particle. This increases in the Cherenkov photon density could be very important for high inclinations, where we can have as much photons as for low inclinations.

Another outstanding item, also shown for all showers energy simulated, is the very low Cherenkov density for γ-ray showers at 80° of zenith angle. Even

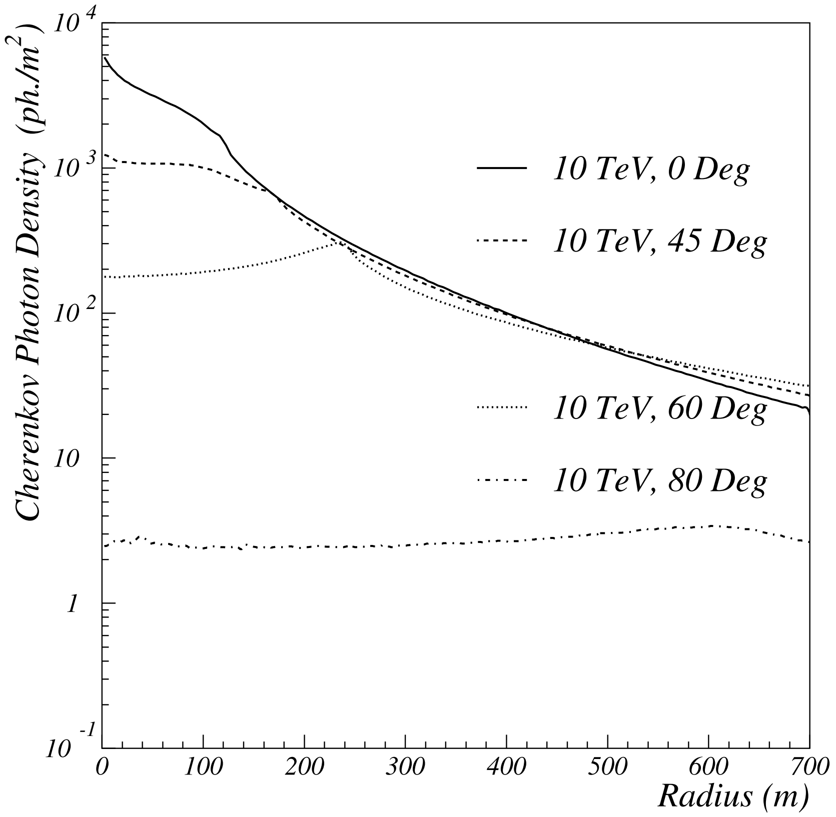

Figure 4.4: *Lateral distribution of Cherenkov light density in 10 TeV γ-ray induced air shower with zenith angles of 0°, 45°, 60°, 80°.*

for 3 TeV or 10 TeV γ-ray showers, this density is very low compared with the same energy γ-ray showers at low zenith angles. In these high zenith angle γ-ray showers, the amount of atmosphere that it has to be crossed is 6 times bigger than for vertical incident showers. As we will see in the next section, this increment in the ray path produce a lose in the Cherenkov light due to the atmospheric attenuation.

4.2 Absorption vs. Wavelength

The large amount of atmosphere traversed by Cherenkov photons produced by HZA showers has also dramatic effects on the wavelength distributions of those photons reaching the ground, as we can see in the figures 4.5, 4.6 and 4.7. For all the energies and zenith angles simulated, we have normalized the absorption curves to a non-absorbed vertical incident γ-ray curve before absorption.

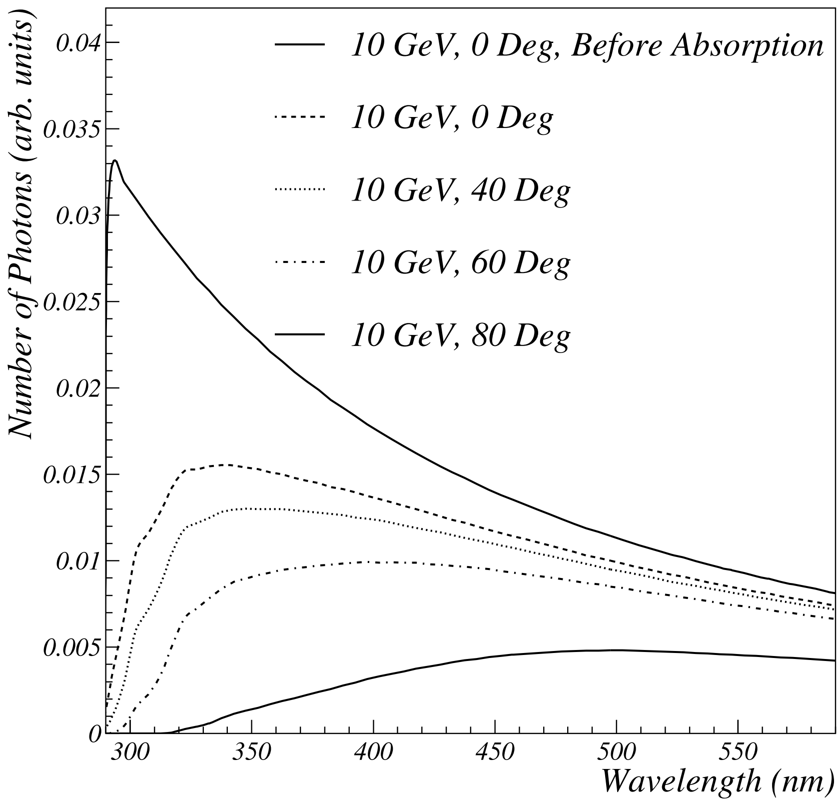

Figure 4.5: *Atmospheric absorption of 10 GeV γ-shower Cherenkov photons as a function of the photons wavelength for different zenith angles.*

The atmospheric attenuation model used to calculate the absorption was explained in the chapter 2. In this model, we calculated the *Rayleigh scattering*, *Aerosol scattering* and *Ozone absorption*, for different altitudes and for different zenith angles using the *air-mass factor*.

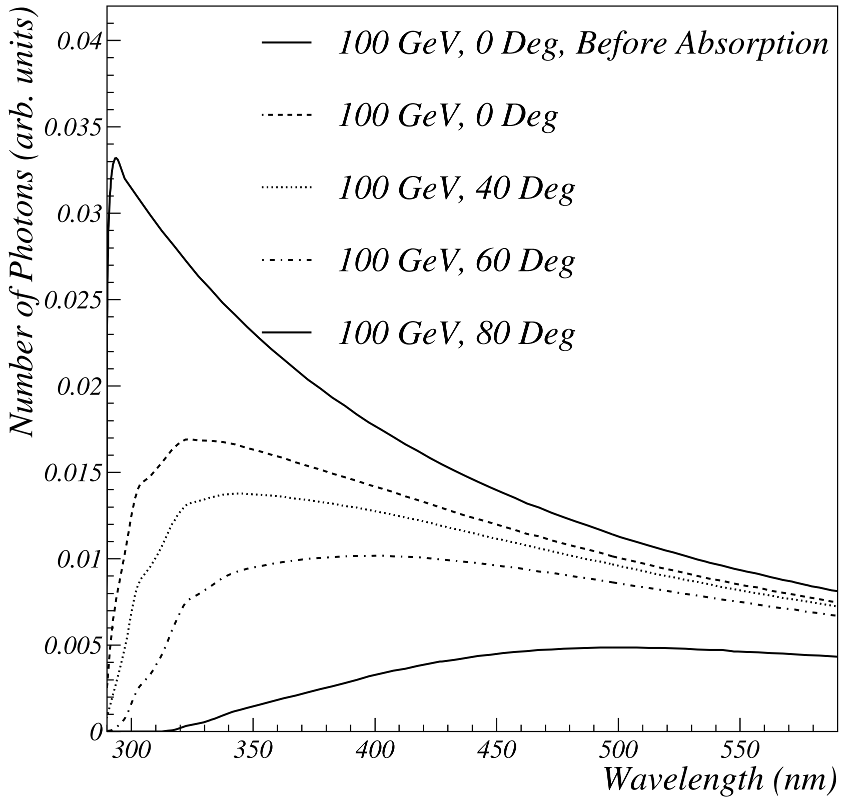

Figure 4.6: *Atmospheric absorption of 100 GeV γ-shower Cherenkov photons as a function of the photons wavelength for different zenith angles.*

As already explained in chapter 2, the *Rayleigh scattering* takes place mainly at low wavelength (it follows a λ^{-4} law). So, the large wavelengths are not affected by *Rayleigh scattering*, and those wavelengths can travel throw the atmosphere without been scattered.

Due to this effect it can be observed that for all the energies the Rayleigh scattering reduce the amount of Cherenkov photons reaching the ground and

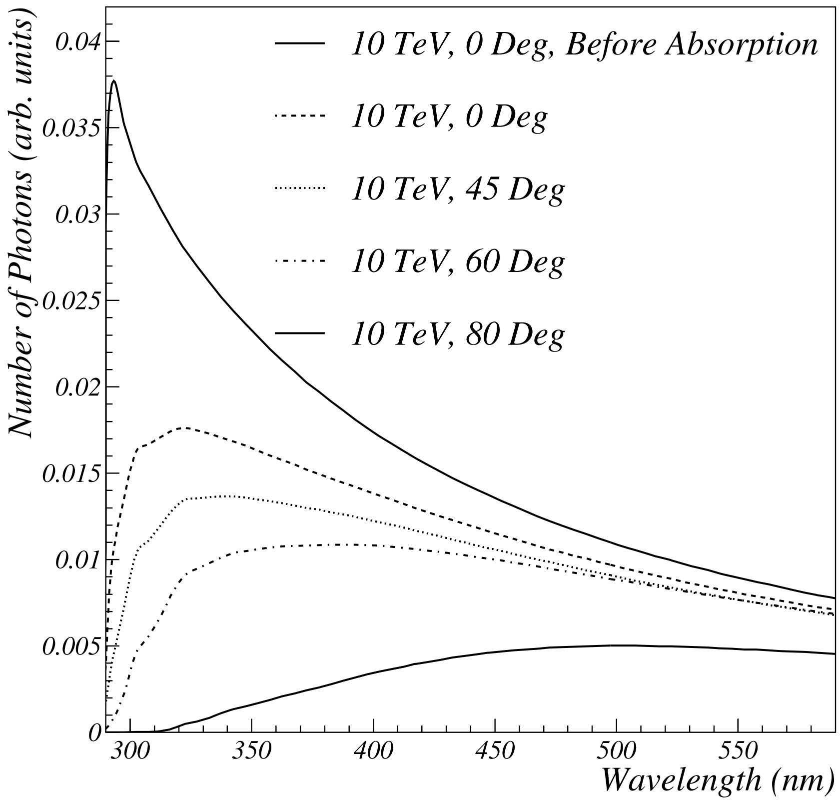

Figure 4.7: *Atmospheric absorption of 10 TeV γ-shower Cherenkov photons as a function of the photons wavelength for different zenith angles.*

shifts the maximum of the wavelength distribution towards red for HZA showers. In the limiting case, for γ-rays arriving at zenith angles around 80°, the maximum of the wavelength distribution peaks at around 500 nm, roughly independent of the energy.

Aerosol effects all wavelength in the same way, execpt in the days of *"calima"* (coming from Sahara dessert during summer). During these conditions, Aerosol scattering becomes impredictible and observations turn meaningless. Fortunately, *"calima* only take place a few days during the year.

By comparing the figures 4.5 and 4.7 with energies of 10 GeV and 10 TeV, respectively, it can be seen a big difference in the amount of Cherenkov photons absorbed for wavelength lower that 330 nm, such that the ozone absorption for 10 GeV showers is higher than for 10 TeV shower.

The maximum Cherenkov photon production for 10 TeV showers happens at a vertical height lower than 8 Km. At this altitudes, the ozone layer has been exceeded (we remember that the ozone layer is located in the Stratosphere, at an altitude around 15 Km), so the ozone absorption at this energies does not take place.

Chapter 5

Conclusions

We performed a detailed study of *γ-ray Extensive Air Showers* up to 80° of zenith angle and for energies between 10 GeV - 10 TeV. The EAS simulations were made with CORSIKA programme.

CORSIKA code was not able to simulate γ-ray showers at high zenith angles so we had to modify it, and introduce a new algorithm in order to simulate γ-ray showers at high zenith angles. When the arriving EAS come with HZA, the atmosphere is thicker than for LZA, so we had to introduce detailed *air-mass* factor.

Due to the increase in the atmospheric thickness, we performed a detailed study of atmospheric absorption which is basic for the knowledge and simulation of the EAS at HZA.

The atmospheric thickness for showers with zenith angle higher than 60° is so large that the shower's Cherenkov photons are almost extinguished. Moreover, for these high zenith angles, small variations in the atmospheric aerosols composition can produce big variations in the Cherenkov light at a ground level.

Also been studied how seasonal changes in the ozone concentration can modify the amount of Cherenkov light in the detector.

The CORSIKA HZA correction and atmospheric absorption has been carefully checked, by studying the electron-positron and Cherenkov photons longitudinal profiles.

The atmospheric attenuation studies for different zenith angles and several energies, show us that when we increase the zenith angle, the maximum in the Cherenkov light spectrum move towards large wavelengths. In the limiting case of 100 GeV EAS with zenith angle of 80°, the maximum transmitted Cherenkov photons occurs at 500 nm wavelength, while, for a 40° zenith angle shower, the maximum is reached at a 330 nm wavelength.

The Cherenkov photon lateral distributions obtained for different zenith angles show reduction in the Cherenkov photon density and *hump* displacement when we increase the zenith angle.

The *hump* displacement seen when we increase the zenith angle it is only due to a geometrical effect of the EAS itself. Moreover, this *hump* movement is the same for γ-ray showers of different energy but with the same zenith angle. For example, γ-ray showers with zenith angle of $0°$ have the *hump's* maximum at 120 m. While, for γ-ray showers with zenith angle of $60°$ have the *hump's* maximum at around 220 m.

From the results obtained in this work, it is inferred that, observing EAS at HZA allow us to enlarge the energetic threshold of the Cherenkov telescopes. Furthermore, if we observe γ-ray sources with Cherenkov telescopes at HZA, the collection area, for EAS detection, increase a lot.

With this technique, we can also observe objects longer, this fact is very useful to study, for example, periodicities in the γ-ray sources.

From all said above we conclude that, although current Cherenkov telescopes can apply the HZA technique, only the next generation of Cherenkov telescopes will take fully advantage of this technique. In order to do so, they will need to incorporate large mirror areas, small size camera pixels and red-extended photosensors.

Bibliography

[1] T. C. Weeks 1985, *The Gamma-Ray Universe*; *Infinite Vistas* Cornell and Carr Editors.

[2] J. V. Jelley and T. C. Weeks 1995, *Ground-Based Gamma-Ray Astronomy*; Sky and Telescope, pag. 20, Sep. 1995.

[3] D. J. Fegan 1997, *γ-hadron separation at TeV energies*; J. Phys. G: Nuclear Part. Phys. **23**: 1013-1060.

[4] J. V. Jelley 1958, *Cherenkov Radiation and its Applications*; Ed. Pergamon Press.

[5] A. M. Hillas 1996, *Differences Between Gamma-Ray and Hadronic Showers*; Space Sciense Reviews **75**: 17-30.

[6] W. R. Leo 1987, *Techniques for Nuclear and Particle Physics Experiments*; Ed. Springer-Verlag.

[7] P. Sokolsky 1988, *Introduction to Ultra High Energy Cosmic Ray Physics*; Ed. Addison-Wesley.

[8] A. M. Hillas 1990, *Characteristics and Brightness of Cerenkov Shower Images for Gamma-Ray Astronomy near 1 TeV*; J. Phys. G: Nucl. Part. Phys. **16**: 1271-1281.

[9] J. Knapp 1997, *High Energy Interactions and Extensive Air Showers*; 25^{th} International Cosmic Ray Conference, Durban, South Africa.

[10] J. Knapp and D. Heck, *Extensive Air Shower Simulation with CORSIKA*; User's Guide, version 5.61 April 1998.

[11] Krennrich, F, et al. 1997, *ApJ* **481**, 758.

[12] D. Heck, J. Knapp, J. N. Capdeville, G. Schatz and T.Thouw 1998, *CORSIKA: A Monte Carlo Code to Simulate Extensive Air Showers.*

[13] *The MAGIC Telescope for Gamma-Ray Astrophysics above 10-30 GeV*; Letter of Intent, June 1998.

[14] A. Konopelko 1998, *The Monte Carlo Characteristics of the HEGRA system of Imaging Air Cherenkov Telescopes. Elsevier preprint*, May 1998.

[15] Nishimura, J. 1967, *Handbuch der Physik* XLVI/2, 1

[16] A. M. Hillas 1985, *Cherenkov Images of EAS Produced by Primary Gamma-Rays and by Nuclei*; Proc. 19^{th} ICRC (La Jolla) **3** 445.

[17] F.A. Aharonian, W. Hofmann, A. K. Konopelko and H.J. Volk 1997, *The potential of Ground Based Arrays of Imaging Atmospheric Cherenkov Telescopes. I. Determination of Shower Parameters*; Astroparticle Physics **6**: 343-368.

[18] M. S. Longair 1992; *High Energy Astrophysics*, Ed. Cambridge Universiy Press.

[19] K. Greisen 1956; Prog. Cosmic Ray Phys. 3.

[20] P. Sommers and J. W. Elbert 1987; *Ultra-High gamma-ray Astronomy Using Atmospheric Cherenkov Detectors at Large Zenith Angles*; J. Phys. G:Nucl. Phys. **13** 553-566.

[21] Tanimori, T, et al. 1998 *ApJ* **492** L33-L66.

[22] Allen, C. W. *Astrophysical Quantities.* Athlone Press editor, 1973.

[23] Benn, C. R. *La Palma night-sky brightness.* ING La Palma Technical note 115. 1998.

[24] Elterman L. *Handbook of geophysics anda space environments, ch. 7.* S. L. Valley editor, NY. 1965.

[25] Hayes, D. and Latham, D. *A rediscussion of the atmospheric extinction and the absolute spectral-energy distribution of Vega.* The Astrophysical Journal, 197: 593-601, 1975.

[26] King, D. *Atmospheric extinction at El Roque de los Muchachos Observatory, La Palma.* ING La Palma Technical Note 31. 1985.

[27] Kondratyev, K. *Radiation in the atmosphere, vol 12.* Academic Press editor, NY. 1969.

[28] McClatchey, R. *Optical properties of the atmosphere.* Handbook of Optics. 1978.

[29] Moulin, C. *Control of atmospheric export of dust from North Africa by the North Atlantic Oscillation.* Nature 387: 691-694, 1997.

[30] Murdin, P. *Geology and meteorology of Sahara dust.* ING La Palma Technical Note 41, 1986.

[31] Murdin, P. *Nightime skies above the Canary Islands.* Vistas In Astronomy, Vol. 28: 449-465, 1985.

List of Figures

List of Tables